UNIVERZITA PALACKÉHO
Přírodovědecká fakulta
Katedra optiky

# Příprava korelovaných párů fotonů a jejich využití v experimentech s kvantovým zpracováním informace

Michal Mičuda

Disertační práce k získání
akademicko-vědeckého titulu doktor (Ph.D.)

Název a číslo vědního oboru: Fyzika P1701
Studijní obor: Optika a optoelektronika

Olomouc 2011

PALACKÝ UNIVERSITY
FACULTY OF NATURAL SCIENCES
Department of Optics

# Generation of correlated photon pairs and their use in quantum information processing experiments

Michal Mičuda

Olomouc   2011

Generation of correlated photon pairs and their use in quantum information processing experiments

# Acknowledgements

First of all, I would like to thank my supervisor Professor Miloslav Dušek for his support and freedom he gave me during my PhD studies. I would like to thank my colleagues and friends Jaromír Fiurášek and Miroslav Ježek for their continuous and generous support and help with solving theoretical and experimental problems. My special thanks belong to Petr Marek for his friendship and unconditional support during my stay at university.

Further, I would like to thank (in alphabetical order) Zdeněk Bouchal, Lucie Čelechovská, Radek Čelechovský, Radim Filip, Jiří Herec, Zdeněk Hradil, Ladislav Mišta, Jaroslav Wagner, and other members of Department of Optics for support. I am also grateful to Martin Hendrych for his guidance during my stay at ICFO.

Finally, my warmest thanks go to my family.


Thank you.

# Contents

# Chapter 1

# Goals of the Thesis

The aim of the thesis is to present my work in the field of generation of correlated photon pairs via spontaneous parametric down-conversion and their applications in quantum information processing experiments.

The first part of the thesis, chapter 2, briefly describes historical and contemporary state of research in the field of photon pairs generation and quantum information processing. The tools and methods important for the rest of this work are described in chapter 3. We review quantization of electromagnetic field, Fock state representation, two photon Hong-Ou-Mandel interference, beam transformation by a diffraction grating, spontaneous parametric down-conversion, and energy and momentum conservation laws and their implications.

The various types of frequency correlations of entangled photon pairs generated via spontaneous parametric down-conversion are studied in chapter 4. With the pulse-front tilt technique we demonstrate experimentally full control of the frequency correlations of entangled photon pairs. The method used to generate different frequency correlations is based on a proper tailoring of the group velocities of all interacting waves in the nonlinear medium through the use of beams with angular dispersion. The medium with angular dispersion, such as a diffraction grating, causes tilting of the pulse front. Chapter 4 contains two different experiments: direct and indirect measurements of frequency correlations, showing possibilities of the mentioned technique. We demonstrate generation of frequency anti-correlated photon pairs entangled in polarization for the case of femtosecond pump beam without any need for narrow filters in front of the detectors. We also show generation of highly frequency correlated photon pairs, which can be used, for example, in some protocols for the quantum enhanced clock synchronization. The last special case is the generation of the frequency uncorrelated photon pairs. It is

worth mentioning that the generated frequency correlations mentioned above are only particular cases of all the correlations and bandwidths that can be achieved with this technique. The technique, we employ, works independently of the wavelength and the nonlinear crystal, and therefore it can be implemented in materials and at wavelengths where conventional solutions are not available.

In chapter 5, we experimentally demonstrate a programmable single-qubit quantum gate. This quantum processor applies a unitary phase shift operation to the data qubit with the value of the phase shift being fully determined by the state of the program qubit. Our linear optical implementation is based on encoding of qubits into polarization states of single photons, two-photon interference on a polarizing beam splitter, and measurement on the output program qubit. We characterize the programmable gate by full quantum process tomography. We show that by using a different set of program states the device can also operate as a programmable partial polarization filter.

In chapter 6 we investigate the optimal discrimination between two projective quantum measurements on a single qubit. We consider a scenario where the measurement that should be identified can be performed twice and we show that adaptive discrimination strategy, entangled probe states, and feed-forward all help to increase the probability of correct identification of the measurement. We also experimentally demonstrate the studied discrimination strategies and test their performance. The employed experimental setup involves projective measurements on polarization states of single photons and preparation of required probe two-photon polarization states by the process of spontaneous parametric down-conversion and passive linear optics.

The main results of the thesis are reviewed in chapter 7, where we also give brief outlook of future work. The list of my publications, citation index and bibliography are given at the end of the thesis. The thesis and all supporting materials are included in the electronic form on the attached CD.

The main chapters of this thesis containing new scientific results are based on the following papers.

M. Hendrych, M. Mičuda, J. P. Torres, *Tunable control of the frequency correlations of entangled photons*, Opt. Lett. **32**, 2339 (2007).

M. Mičuda, M. Ježek, M. Dušek, J. Fiurášek, *Experimental realization of a programmable quantum gate*, Phys. Rev. A **78**, 062311 (2008).

M. Hendrych, M. Mičuda, A. Valencia, J. P. Torres, *Photons with tunable spectral shapes: The transition from frequency anticorrelated to correlated photon pairs*, eprint: arXiv:0908.1857v1 [quant-ph] (2009).

J. Fiurášek, M. Mičuda, *Optimal two-copy discrimination of quantum measurements*, Phys. Rev. A **80**, 042312 (2009).

# Chapter 2

# Contemporary state of research

The discovery of the laser in 1960 enabled rapid development in the field of nonlinear optics. This discipline involves every phenomena where light interacts with light via a nonlinear medium. Every medium can behave in a nonlinear way if sufficient intensity of light is applied. The results of this nonlinear behavior are, for example, dependance of refraction index on optical intensity,[1] controlling light via light,[2] or optical frequency conversion.[3]

Very interesting applications of nonlinear optics are sources generating light with nonclassical properties such as entanglement. Correlations of entangled particles are much stronger than the classical ones and can be verified by Bell test measurement.[4] The most widely used method for the generation of pairs of entangled photons is spontaneous parametric downconversion (SPDC) where two lower-frequency photons are generated when a strong pump field interacts with a nonlinear medium. The generated photons can be correlated and entangled in various degrees of freedom such as polarization,[5] frequency,[6] and orbital angular momentum.[7,8] To measure the quality of the source we often employ Hong-Ou-Mandel effect.[9] This effect is based on two photon interference. If two incident photons are indistinguishable and arrive at the same time and the same spot at the balanced beam splitter, then both photons leave in the same output mode.

To date, most quantum information applications use the polarization of photons, or polarization entanglement between photon pairs, as a quantum resource. However, the spectrum of the photons can be considered a quantum resource by itself. To faithfully describe frequency entanglement one needs to use infinite dimensional Hilbert space. This offers a possibility of implementing quantum algorithms employing the high dimensional Hilbert space either because it is required by the nature of quantum state (qudits) or because it is associated with advantage in the

form of enhanced efficiency. Furthermore, the frequency properties of entangled two-photon states cannot be neglected even when entanglement takes place in the polarization or spatial degrees of freedom. In this case, the corresponding entangled states make use only of a portion of the total two-photon quantum state, and any frequency correlations therefore supply a "which path" information and degrade the degree of entanglement.

The optimal bandwidth, as well as the most appropriate type of frequency correlations between paired photons, depends on the specific quantum information application we consider. Atom-photon interfaces address specific atomic transitions that require ultra-narrow-band quantum light ($\sim$ MHz), while the generation of ultrahigh fluxes of entangled photons ($\sim \mu$W) with nonclassical properties requires light with largely enhanced bandwidth ($\sim$ tens of nm).[10,11] Some protocols for quantum enhanced clock synchronization and position measurement rely on use of frequency correlated photons.[12] Heralded single photons with a high degree of quantum purity can be obtained by generation of uncorrelated paired photons. The tolerance against the effects of mode mismatch in linear optical circuits, the dominant cause of photon distinguishability, can be enhanced by using photons with appropriately tailored wave-packet shape.[13]

The most common configuration for the source of photon pairs uses continuous wave pumping producing frequency anticorrelated photons. Other specific frequency correlations, such as correlated or uncorrelated photons, can occur in special crystals with suitable pump light conditions, specific values of the nonlinear crystal length and dispersive properties of the nonlinear crystals.[14,15] One strategy for engineering the bandwidth is based on the proper preparation of the downconverting crystal. Frequency-entangled pairs of photons with a largely enhanced bandwidth can be generated in chirped quasi-phase-matched nonlinear crystals,[16] while paired photons with a largely reduced spectral width can be generated in cavity SPDC.[17] Properly designed SPDC configurations with nonlinear crystal superlattices allow tailoring the frequency correlations of paired photons.[18]

In general, noncollinear SPDC geometries allow control of the bandwidth of downconverted photons as well as of the waveform.[19] SPDC configurations, where the downconverted photons counter-propagate, allow reducing the spectral width of light.[20,21] Noncollinear SPDC allows the generation of frequency-correlated and uncorrelated photons by controlling the pump beam width and the angle of emission of the downconverted photons.[22,23]

Huge drawback of sources based on SPDC is their limited scalability. With the

state of art technology it is unfeasible to generate more than four pairs of photons.[24] Nevertheless states of light are less susceptible to decoherence because of weak interaction strength with environment. This feature of photons is widely explored in quantum information applications where the ultimate goal is to build a quantum computer. Quantum computer[25–27] promises computational power beyond what classical computers can offer. There are several areas where quantum computers offers speedup and can be effectively used to solve problems, such as searching over a large database,[28] large number factorization[29] or efficient simulation of quantum systems.[30] Quantum computer, like its classical counterpart, can be constructed from elementary blocks called gates. One of the most important logic gate for classical computer is the Toffoli gate.[30] The Toffoli gate is universal reversible three-qubit gate,[31] sometimes called Controlled-Controlled-NOT, which applies the NOT operation on the target qubit conditionally on logical states of two control qubits. Quantum counterpart of the Toffoli gate is also reversible and with the combination with one-qubit Hadamard gate gives an universal quantum gate set.[32] Three-qubit quantum gates play important role in quantum error correction[33] and fault tolerance.[34] Nevertheless, three-qubit quantum gates are not elementary and can be decomposed into two-qubit quantum gates[25,35,36] which are universal for quantum computation.

One of the earliest proposals for implementing quantum computation[37] used qubits, each of which represented by a single photon in two optical modes. The major obstacle for experimental demonstration was the difficulty of realizing the nonlinear interactions between photons, which are needed for the implementation of two-qubit operations. This obstacle was overcame by Knill, Laflamme and Milburn (KLM) in 2001, using linear optical elements, ancilla photons and post-selection.[38] They used measurement to nondeterministically realize the optical nonlinearity required for two-qubit entangling gates. Moreover, they also showed that probability of success of those nondeterministic quantum gates can be increased arbitrarily close to one. Since then, there has been tremendous effort in theoretical development of linear optics schemes[39–47] and their experimental realizations.[48–65] Also note that there are many other physical systems explored experimentally to create universal quantum gates besides photons, such as atoms,[66,67] ions,[68–70] superconducting circuits[71,72] or nuclear magnetic resonance.[73–76]

Quantum computation requires the ability to perform arbitrary unitary operations on a set of quantum states. Each unitary operation can be constructed as an array of elementary gates.[36] But one can take inspiration from classical computers,

where the gate array is fixed and program specifies the operation to be performed on the data. It is intriguing to attempt to generalize this concept to quantum computing.[30]

Unfortunately, Nielsen and Chuang in their seminal paper[77] proved that it is not possible to build a deterministic universal quantum gate array. They showed that an $n$ qubit quantum register can perfectly encode at most $2^n$ distinct quantum operations. Nevertheless it is possible to construct approximate programmable quantum gates and optimize their performance for a given size of the program register.[78–83] There are two complementary strategies one can pursue. One strategy designs gates that always deterministically provide an output, but add some noise to the output states.[83] The second strategy avoids the extra noise at a cost of reduced probability of success.[77–79] These gates involve measurements whose outcomes herald success or failure. The single-qubit programmable quantum measurement devices,[84–93] where the state of program qubit determines the measurement on data qubit, were implemented for single-photons[94] and for nuclear spins in a nuclear magnetic resonance experiment.[95] Moreover, a programmable discriminator of coherent states was realized[96,97] and also programmable unitary quantum gate for photonic qubits has been reported.[62] Note that there is an alternative to the traditional circuit-based approach, called the cluster-state model of quantum computing, or one-way quantum computing.[98,99] This model is based on employing an entangled multi-qubit quantum state, where the input state is encoded into some qubits. Proper measurements and feed forward are used to evolve the quantum state and "teleport" it towards the desired final state, which is than measured to complete the computation.

# Chapter 3

# Methods and tools

## 3.1 From classical to quantum

Light as an electromagnetic field is described by electric and magnetic intensity vectors $\vec{E}(\vec{r},\,t)$ and $\vec{H}(\vec{r},\,t)$ which obey Maxwell equations.[101] For the electromagnetic field in free space the electric intensity vector $\vec{E}$ (or magnetic intensity vector $\vec{H}$) satisfies the wave equation

$$\nabla^2\vec{E} - \frac{1}{c^2}\frac{\partial^2\vec{E}}{\partial t^2} = 0, \tag{3.1}$$

where $c$ is speed of light and $t$ is time. Consider the radiation field in a large finite cubic cavity of volume $V$. Linearity of the equation (3.1) allow to express the electric intensity vector $\vec{E}(\vec{r},\,t)$ in form

$$\vec{E}(\vec{r},\,t) = \sum_k \sqrt{\left(\frac{\hbar\nu_k}{2\varepsilon_0 V}\right)}[\alpha_k e^{-i2\pi\nu_k t}\vec{u}_k(\vec{r}) + \alpha_k^* e^{i2\pi\nu_k t}\vec{u}_k^*(\vec{r})], \tag{3.2}$$

where $\hbar$ is the reduced Planck constant, $\nu_k$ is mode frequency, $\varepsilon_0$ is free space permittivity, $\alpha_k$ is classical complex amplitude, $\vec{u}_k(\vec{r})$ is mode function satisfying equation (3.1) and boundary conditions. Electromagnetic field can be intuitively described as an ensemble of simple electromagnetic oscillators. The study of the quantum features of the light requires the quantisation of the electromagnetic field.[102, 103] This is accomplished by substitution in equation (3.2) $\alpha_k \rightarrow \hat{a}_k$ and $\alpha_k^* \rightarrow \hat{a}_k^\dagger$, respectively. The electric field operator reads

$$\hat{E}(\vec{r},\,t) = \hat{E}^+(\vec{r},\,t) + \hat{E}^-(\vec{r},\,t) = \sum_k \sqrt{\left(\frac{\hbar\nu_k}{2\varepsilon_0 V}\right)}[\hat{a}_k e^{-i2\pi\nu_k t}\vec{u}_k(\vec{r}) + \hat{a}_k^\dagger e^{i2\pi\nu_k t}\vec{u}_k^*(\vec{r})], \tag{3.3}$$

where operators $\hat{E}^+(\vec{r}, t)$ and $\hat{E}^-(\vec{r}, t)$ refer to the positive and negative frequency part of the electric field operator, respectively. Positive and negative frequency part of the electric field operator are related by $\hat{E}^+(\vec{r}, t) = [\hat{E}^-(\vec{r}, t)]^\dagger$. Operator $\hat{a}^\dagger$ is called creation operator and represents creation of one photon in a given mode of electromagnetic field. Operator $\hat{a}$ represents annihilation of one photon in the given mode of electromagnetic field and is called annihilation operator. Since operators $\hat{a}^\dagger$ and $\hat{a}$ represent photons therefore they obey bosonic commutations relations

$$[\hat{a}_k, \hat{a}_{k'}] = [\hat{a}_k^\dagger, \hat{a}_{k'}^\dagger] = 0, \quad [\hat{a}_k, \hat{a}_{k'}^\dagger] = \delta_{k, k'}. \tag{3.4}$$

With the aid of operators $\hat{a}^\dagger$ and $\hat{a}$ we can define photon number operator

$$\hat{n}_k = \hat{a}_k^\dagger \hat{a}_k, \tag{3.5}$$

which describes number of photons in the particular field mode.

## 3.2   Fock states representation

Fock states are defined as eigenstates of the number operator

$$\hat{n}|n\rangle = n|n\rangle, \tag{3.6}$$

where $n$ is real number. For the normalized Fock state $|n\rangle$, it holds

$$|n\rangle = \frac{\hat{a}^{\dagger n}}{\sqrt{n!}}|0\rangle. \tag{3.7}$$

Fock states are orthonormal

$$\langle n|m\rangle = \delta_{n, m} \tag{3.8}$$

and copmlete

$$\sum_{n_k=0}^{\infty} |n_k\rangle\langle n_k| = \hat{1}. \tag{3.9}$$

Fock states form a complete set of basis vectors in the Hilbert space and every state can be described in terms of the Fock states. For creation and annihilation operators holds

$$\hat{a}^\dagger |n\rangle = \sqrt{n+1}\,|n+1\rangle \tag{3.10}$$

$$\hat{a}\,|n\rangle = \sqrt{n}\,|n-1\rangle \tag{3.11}$$

and vacuum stability condition requires that $\hat{a}\,|0\rangle = 0$.

## 3.3    Hong-Ou-Mandel interference

Hong-Ou-Mandel (HOM) effect is phenomenon where two photons interfere on the beam splitter. If incident photons are indistinguishable and arrive at the same time and place at the beam splitter then both photons leave in the same output mode.[9]

To illustrate this phenomenon, let us consider lossless beam splitter with $\hat{a}_{in}^{\dagger}$, $\hat{b}_{in}^{\dagger}$ input mode operators and $\hat{a}_{out}^{\dagger}$, $\hat{b}_{out}^{\dagger}$ output mode operators. The beam splitter transformation of the input modes in Heisenberg picture can be written as

$$\hat{a}_{in}^{\dagger} = t\hat{a}_{out}^{\dagger} + r\hat{b}_{out}^{\dagger} \qquad \text{and} \qquad \hat{b}_{in}^{\dagger} = t\hat{b}_{out}^{\dagger} - r\hat{a}_{out}^{\dagger}, \tag{3.12}$$

where $t$ and $r$ are real amplitude transmissivity and reflectivity, respectively.

Let's assume for the simplicity that we have only one photon in each input arm of the beam splitter and input state is

$$|\varphi\rangle_{in} = \hat{a}_{in}^{\dagger}\hat{b}_{in}^{\dagger}|0,0\rangle. \tag{3.13}$$

The transformation of the input state $|\varphi\rangle_{in}$ by beam splitter yields

$$\begin{aligned} |\varphi\rangle_{in} \Rightarrow |\varphi\rangle_{out} &= (t\hat{a}_{out}^{\dagger} + r\hat{b}_{out}^{\dagger})(t\hat{b}_{out}^{\dagger} - r\hat{a}_{out}^{\dagger})|0,0\rangle \\ &= (t^2 - r^2)|1,1\rangle + \frac{tr}{\sqrt{2}}(|0,2\rangle - |2,0\rangle). \end{aligned} \tag{3.14}$$

For balanced beam splitter $t = r = \frac{1}{\sqrt{2}}$ term $|1,1\rangle$ is equal to zero and both photons simultaneously exit the same output port of the beam splitter. We can see from equation (3.14) that output $a$ and $b$ are equally probable. If we measure with detector at each output port seeking for positive detection event at both detectors at the same time, i. e. we perform coincidence measurement, we will see no simultaneous detection events.

The quality of the HOM effect can be characterized by interference visibility $V$ on the beam splitter. Visibility is defined

$$V = \frac{R_{max} - R_{min}}{R_{max} + R_{min}}, \tag{3.15}$$

where $R_{max}$ and $R_{min}$ are maximum and minimum number of coincidences, respectively.

## 3.4    Beam transformation by the diffraction grating

Diffraction grating is an optical element with periodic structure which diffracts incoming light into one or more beams traveling in various directions. Incident and diffracted beams are related by grating equation

$$\sin(\theta_i) + \sin(\theta_m) = \frac{m\lambda}{d}, \tag{3.16}$$

where $\theta_i$ is the angle of incidence at grating, $\theta_m$ is the output diffraction angle, $m$ is order of the diffraction, $\lambda$ is wavelength and $d$ groove spacing of the grating.



Figure 3.1: Diffraction grating, where incoming beam propagating in direction $\vec{k}_0$ and $\vec{k}$ are diffracted to the $m^{\text{th}}$ diffraction mode in $\vec{k}_{m0}$ and $\vec{k}_m$ directions.

Consider now non-monochromatic light beam with central angular frequency $\omega_0$ which propagates in the $z$ direction. The main direction of propagation is defined by $\vec{k}_0$. Deviations from the central frequency and main direction of propagation for the incident beam, see Fig. 3.1, can be written

$$\Omega = \omega - \omega_0 \quad \text{and} \quad \Theta_i = \theta_i - \theta_{i0}. \tag{3.17}$$

The deviation of the diffracted angle $\Theta_m = \theta_m - \theta_{m0}$, according to Eq. (3.16), depends not only on angle of incidence $\theta_i$ but also on the angular frequency $\omega$. The approximate solution for diffracted angle deviation can be found by Taylor expansion of the grating Eq. (3.16) to the first order[104] which yields

$$\Theta_m = \alpha\Theta_i + \beta\Omega, \tag{3.18}$$

where $\alpha = -\frac{\cos(\theta_{i0})}{\cos(\theta_{m0})}$ and $\beta = -\frac{m\lambda_0^2}{2\pi c d \cos(\theta_{m0})}$. The $x$ component of the vector $\vec{k}$ describing incident beam can be written $p_x = |\vec{k}|\Theta_i$. Similarly, for the $x$ component

of the vector $\vec{k}_m$ describing diffracted beam we can write with the help of (3.18)

$$
\begin{aligned}
p_{x,m} &= |\vec{k}|\Theta_m = |\vec{k}|\alpha\Theta_i + \beta\Omega \\
&= \alpha p_x + \beta|\vec{k}|\Omega = \alpha p_x + \beta|\vec{k}_0|\Omega,
\end{aligned}
\tag{3.19}
$$

where we did Taylor expansion of the $|\vec{k}|$ and neglected the second and higher orders. Eq. (3.19) shows transformation of the $x$ component of the $\vec{k}$ by diffraction grating. Note here, that light beam always propagates in the $z$ direction. The transformation of the beam amplitude by diffraction grating is

$$
E(p_x, p_y, k_z, \omega) \rightarrow E\left(\frac{p_x}{\alpha} - \frac{k_0\beta}{\alpha}\Omega, p_y, k_z, \omega\right) = E\left(\frac{p_x}{\alpha} + \frac{\lambda_0\epsilon}{\alpha c}\Omega, p_y, k_z, \omega\right), \tag{3.20}
$$

where $\epsilon = \frac{m}{d\cos(\theta_{m0})}$ is the angular dispersion and $c$ is speed of light.

## 3.5 Spontaneous parametric down-conversion

The most widely used method for the generation of pairs of entangled and correlated photons is spontaneous parametric down-conversion (SPDC). This process consists in interaction between a nonlinear medium and strong electromagnetic field called pump. When strong pump field interacts with a nonlinear medium one photon from pump field can be converted into two lower-frequency photons called signal and idler. Energy and momentum of signal and idler photons sum up to energy and momentum of the pump photon while nonlinear medium is left unchanged. Properties of generated photons depend on nature of the pump field (e.g. continuous-wave or pulse pumping), geometry of he setup (collinear or non-collinear) and phase matching conditions (type I, type II, etc.). This can result in signal and idler photons being entangled in polarization or spin angular momentum,[5] in frequency,[6] and in orbital angular momentum.[7,8]

The effective Hamiltonian for the three mode SPDC process in the interaction picture is given by

$$
\hat{H}_I(t) = \varepsilon_0 \int_V \chi^{(2)} \hat{E}_p^+(\vec{r}, t)\hat{E}_s^-(\vec{r}, t)\hat{E}_i^-(\vec{r}, t)dV + H.c., \tag{3.21}
$$

where $\varepsilon_0$ is the permittivity of free space, $\chi^{(2)}$ is the second order nonlinear susceptibility tensor, $V$ is the volume of the nonlinear medium, $t$ is time, and $H.c.$ means the Hermitian conjugate. Nonlinear medium illuminated in the $z$ direction

by strong pump beam is described by electric field operator $\hat{E}_p$, which is treated classically. Positive frequency part of the electric field operator is given by[105]

$$\hat{E}_p^+(\vec{x}, z, t) = \int d\omega_p d\vec{p}_p E(\vec{p}_p, \omega_p) \exp\{i(k_p z + \vec{p}_p[\vec{x} + z\vec{\rho}_p] - \omega_p t)\}, \qquad (3.22)$$

where $\omega_p$ is angular frequency of the pump beam, $\vec{p}_p = (p_x, p_y)$ is the transverse momentum, $E(\vec{p}_p, \omega_p)$ is the classical amplitude of the pump field, $\vec{x} = (x, y)$ is the position in the transverse plane, $k_p(\vec{p}_p, \omega_p) = \sqrt{(\frac{\omega_p n_p}{c})^2 - |\vec{p}_p|^2}$ is the longitudinal wave number inside the nonlinear medium, $n_p$ is the refractive index at the pump wavelength, and $\vec{\rho}_p = (\rho_{px}, \rho_{py})$ is the Poynting vector walk-off parameter of the pump beam due to the different propagation directions of the energy and phase fronts inside the anisotropic nonlinear medium. Operator $\hat{E}_j^-$ refer to the negative frequency part of the signal ($j = s$) and idler ($j = i$) electric field operators and are given

$$\hat{E}_j^-(\vec{x}, z, t) \propto \int d\omega_j d\vec{p} \, \hat{a}_j^\dagger(\vec{p}_j, \omega_j) \exp\{-i(k_j z + \vec{p}_j[\vec{x} + z\vec{\rho}_j] + \omega_j t)\}, \qquad (3.23)$$

where $\omega_j$ is angular frequency of the $j^{\text{th}}$ beam, $\vec{p}_j = (p_x, p_y)$ is the transverse momentum, $\hat{a}_j^\dagger(\vec{p}_j, \omega_j)$ is the creation operator for the $j^{\text{th}}$ field, $k_j(\vec{p}_j, \omega_j) = \sqrt{(\frac{\omega_j n_j}{c})^2 - |\vec{p}_j|^2}$ is the longitudinal wave number inside the nonlinear medium, $n_j$ is the refractive index at the $j^{\text{th}}$ wavelength, and $\vec{\rho}_j = (\rho_{jx}, \rho_{jy})$ is the Poynting vector walk-off parameter of the $j^{\text{th}}$ beam in the anisotropic nonlinear medium.

The calculation of the two-photon quantum state within the first order of the perturbation theory gives

$$|\Psi\rangle = |0, 0\rangle - \frac{i}{\hbar} \int_{-\infty}^{\infty} dt \hat{H}_I(t)|0, 0\rangle, \qquad (3.24)$$

where $|0, 0\rangle$ is the vacuum state for the signal and idler mode.

## 3.6   Energy and momentum conversion laws for SPDC

The energy and momentum conversion laws for the SPDC process can be written in the form

$$\omega_p = \omega_s + \omega_i \qquad (3.25)$$
$$\vec{k}_p = \vec{k}_s + \vec{k}_i, \qquad (3.26)$$

where $\omega_j$ and $\vec{k}_j$ are angular frequency and wave vector of the $j^{\text{th}}$ field, where $j = p, s, i$ denotes pump, signal and idler field, respectively.

Let us show one consequence of the Eq. (3.25) and (3.26). Consider now, for the simplicity, collinear SPDC process pumped by monochromatic continuous-wave laser at angular frequency $\omega_p$. One photon from pump field is converted into two different lower-frequency photons at angular frequencies $\omega_s$ and $\omega_i$, let say that $\omega_s \geq \omega_i$. The Eq. (3.26) can be rewritten

$$\omega_p n(\omega_p) = \omega_s n(\omega_s) + \omega_i n(\omega_i), \tag{3.27}$$

where $n(\omega_j)$ is refractive index at frequency $\omega_j$. If we express $\omega_i$ from the Eq. (3.25) and put it into Eq. (3.27) we get

$$n(\omega_p) - n(\omega_i) = (n(\omega_s) - n(\omega_i))\frac{\omega_s}{\omega_p}. \tag{3.28}$$

For the medium with normal dispersion holds

$$\omega_i \leq \omega_s \leq \omega_p \quad \text{and} \quad n(\omega_i) \leq n(\omega_s) \leq n(\omega_p) \tag{3.29}$$

and Eg. (3.28) can not be satisfied. Only birefringent medium can fulfill Eg. (3.28) and this is reason why mostly uniaxial or biaxial optical medium are used for the SPDC processes.

Eq. (3.26) is often rephrased to equation

$$\Delta_k = \vec{k}_p - \vec{k}_s - \vec{k}_i, \tag{3.30}$$

where $\Delta_k$ is called phase mismatch. Eq. (3.30) is called phase-matching condition. The intensity of the SPDC process is limited by

$$I \approx sinc^2 \left( \frac{\Delta_k L}{2} \right), \tag{3.31}$$

where $L$ is length of the nonlinear medium.

Consider now, collinear SPDC process with broadband pump field. The angular frequency of all interacting fields in the medium can be written $\omega_j = \omega_{0j} + \Omega_j$, where $j = p, s, i$ denotes pump, signal and idler field, respectively.

Let assume that relation between central angular frequency $\omega_{0j}$ and angular frequency deviation $\Omega_j$ is $\omega_{0j} \gg \Omega_j$. To gain maximum intensity of the SPDC process Eq. (3.30) must be equal to zero for all angular frequencies interacting in

the nonlinear crystal. Eq. (3.25) and (3.26) can be now rewritten in the form of

$$
\begin{aligned}
\omega_p &= \omega_s + \omega_i \\
\omega_{0p} &= \omega_{0s} + \omega_{0i} \\
\Omega_p &= \Omega_s + \Omega_i \\
k_p(\omega_p) &= k_s(\omega_s) + k_i(\omega_i).
\end{aligned}
\tag{3.32}
$$

The phase mismatch Eq. (3.30) can be expand into Taylor series around the central angular frequencies $\omega_{0j}$ and we get

$$
\begin{aligned}
\Delta_k &= \sum_{l=0}^{\infty} \frac{1}{l!} \frac{\partial k_p^l}{\partial \omega_p^l}\bigg|_{(\omega_{0p})} (\Omega_p)^l - \sum_{l=0}^{\infty} \frac{1}{l!} \frac{\partial k_s^l}{\partial \omega_s^l}\bigg|_{(\omega_{0s})} (\Omega_s)^l - \sum_{l=0}^{\infty} \frac{1}{l!} \frac{\partial k_i^l}{\partial \omega_i^l}\bigg|_{(\omega_{0i})} (\Omega_i)^l \\
&= k_p(\omega_{0p}) - k_s(\omega_{0s}) - k_i(\omega_{0i}) + N_p \Omega_p - N_s \Omega_s - N_i \Omega_i + \\
&+ \frac{1}{2} \left[ D_p \Omega_p^2 - D_s \Omega_s^2 - D_i \Omega_i^2 \right] + ...,
\end{aligned}
\tag{3.33}
$$

where $N_j = \frac{\partial k_j}{\partial \omega_j}\big|_{(\omega_{0j})}$ represents inverse group velocity and $D_j = \frac{\partial^2 k_j}{\partial \omega_j^2}\big|_{(\omega_{0j})}$ represents inverse group velocity dispersion. Generally, we limit ourselves to the second order of the Taylor expansion of Eq. (3.33).

# Chapter 4

# Tunable control of the frequency correlations of entangled photons

The motivations to control the joint spectrum of paired photons come from both the applied and fundamental points of view. Frequency-uncorrelated photons are desired because they provide a source of heralded pure single photons, an important tool in quantum computing and communications.[106,107] On the other hand, frequency-correlated and anticorrelated photons are important for quantum metrology, because these types of correlations can enhance the precision of some existing time measurement and synchronization techniques.[108–110] Moreover, the possibility to generate symmetric spectral shapes of entangled photons guarantees that all the distinguishing information that may come from the spectra of the photons is erased. This is a key issue when considering applications based on interferometric techniques, where any distinguishability reduces the visibility of the interference pattern.[111–113]

The search for a way to control the joint spectrum of paired photons has been of paramount importance in the past few years. In particular, techniques based on the choice of specific materials and wavelengths have been used to obtain frequency-uncorrelated[114] and frequency-correlated photons.[115] Experiments that allow a tunable control of the joint spectrum have also been reported.[116–118]

## 4.1   Pulse front tilt technique and SPDC

In this section we will show how pulse front tilt (PFT) technique can affect frequency correlations of entangled photon pairs. The control over the joint spectrum

is based on the possibility of modifying phase mismatch $\Delta_k$ by introducing angular dispersion into the pump and the downconverted beams. The introduction of angular dispersion enables us to tune the frequency characteristics of paired photons by manipulating the transverse momentum.

Let us consider a collinear type II SPDC configuration in uniaxial second order nonlinear crystal of the length $L$. The optic axis of the crystal is contained in the $XZ$ plane. Laser pump beam at angular frequency $\omega_p = \omega_{0p} + \Omega_p$ propagating in the $z$ direction is described by Eq. (3.22), so that $\vec{\rho_p} = (\rho_p, 0)$. The pump beam is diffracted by diffraction grating oriented in the $x$ direction placed in the front of the nonlinear crystal so that each angular frequency component is dispersed in a different direction. The transformation of the pump beam amplitude $E(p_x, p_y, \omega_{0p} + \Omega_p)$ due to the diffraction grating, see chapter 3.4, can be written as

$$E(p_x, p_y, \omega_{0p} + \Omega_p) \rightarrow E\left(\frac{p_x}{\alpha} - \frac{\tan(\xi)}{\alpha c}\Omega_p, p_y, \omega_{0p} + \Omega_p\right). \qquad (4.1)$$

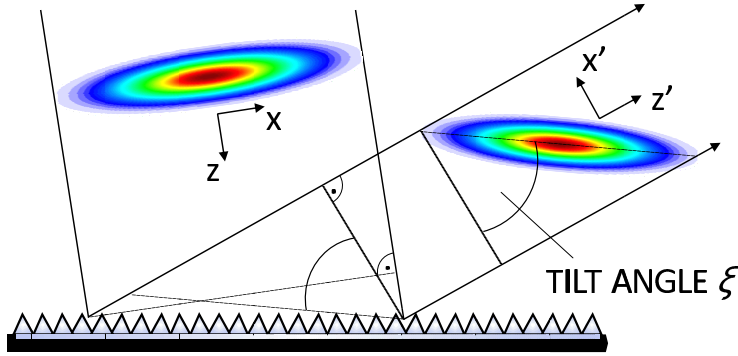When angular dispersion is applied to a pulse, it causes the front of the pulse to



Figure 4.1: Angular dispersion tilts the front of a pulse by an angle $\xi$. After the element that introduces angular dispersion (prism or grating), the pulse front is no longer perpendicular to the direction of propagation. Colors refer to the intensity profile of the front of the pulse.

be tilted by an angle $\xi$, see Fig. 4.1. It means that the front of the pulse acquires a temporal delay that depends on its transversal coordinate.[119] The tilt angle is $\tan(\xi) = -\lambda_{0p}\epsilon$, where $\epsilon = m/(d\cos(\theta_{m0}))$ is the angular dispersion with $d$ being the groove spacing of the grating, $m$ the diffraction order and $\lambda_{0p} = 2\pi c/\omega_{0p}$.

The electric field operator for the signal and idler photon is given by Eq. (3.23). For the configuration mentioned above the walk-off parameter for signal and idler wave is $\vec{\rho_s} = (\rho_s, 0)$ and $\vec{\rho_i} = (0, 0)$. At the output face of the nonlinear crystal

$(z = L)$, a second grating is used to re-collimate the beam by compensating for the angular dispersion introduced by the first grating. The tilt of the pump beam is transferred to the mode function of the downconverted photons and to remove it we must employ another diffraction grating with parameters[104] $\alpha' = 1/\alpha$ and $\epsilon' = -\epsilon/\alpha$. The transformation of the transverse momentum $\vec{p}_j$ of the two photon state function is similar as in the transformation of the pump beam amplitude and yields

$$
\begin{aligned}
\vec{p}_s &= (p_{sx}, p_{sy}) \rightarrow (\overline{p}_{sx}, p_{sy}) = (\alpha p_{sx} + \Omega_s \tan \xi / c, p_{sy}) \\
\vec{p}_i &= (p_{ix}, p_{iy}) \rightarrow (\overline{p}_{ix}, p_{iy}) = (\alpha p_{ix} + \Omega_i \tan \xi / c, p_{iy}).
\end{aligned}
\tag{4.2}
$$

We made assumption that the dispersive gratings act only as dispersive elements. The quantum state of the downconverted photons at the output face of the nonlinear crystal reads

$$
|\Psi\rangle = \int d\vec{p}_s d\vec{p}_i d\omega_s \omega_i \, \Phi(\vec{p}_s, \vec{p}_s, \omega_s, \omega_i) \hat{a}_s^\dagger(\vec{p}_s, \omega_s) \hat{a}_i^\dagger(\vec{p}_i, \omega_i)|0, 0\rangle,
\tag{4.3}
$$

where two photon state function is[105]

$$
\Phi(\vec{p}_s, \vec{p}_i, \omega_s, \omega_i) = E(\vec{p}_s + \vec{p}_i, \omega_s + \omega_i) \mathrm{sinc}\left(\frac{\Delta_k L}{2}\right) \exp\left\{\frac{i\Delta_k L}{2}\right\},
\tag{4.4}
$$

where

$$
\begin{aligned}
\Delta_k &= k_p(\overline{p}_{sx} + \overline{p}_{ix}, p_{sy} + p_{iy}, \omega_s + \omega_i) + (\overline{p}_{sx} + \overline{p}_{ix}) \tan(\rho_p) \\
&\quad - k_s(\overline{p}_{sx}, p_{sy}, \omega_s) - \overline{p}_{sx} \tan(\rho_s) - k_i(\overline{p}_{ix}, p_{iy}, \omega_i).
\end{aligned}
\tag{4.5}
$$

Eq. (4.4) describes an entangled state in both, the signal and idler transverse wavenumber $(\vec{p}_s, \vec{p}_i)$ and signal and idler frequency $(\omega_s, \omega_i)$.

Generally, when we are interested in the frequency properties of paired photons, the light beams are projected into single modes by, for example, coupling the light into singlemode fibers. All the information concerning the frequency correlations of paired photons with frequencies $\omega_j$ can thus be obtained from the joint spectrum, or biphoton, of the two photon state, $\Phi(\vec{p}_s = 0, \vec{p}_i = 0, \omega_s, \omega_i) \equiv \Phi(\omega_s, \omega_i)$.[111–113] The joint spectral intensity, which corresponds to the probability of detecting a photon with frequency $\omega_s$ in coincidence with the other photon with frequency $\omega_i$, writes $S(\omega_s, \omega_i) = |\Phi(\omega_s, \omega_i)|^2$.

The introduction of angular dispersion into the pump and the down converted photons results in an effective inverse group velocity $N_j'$ and effective inverse group

velocity dispersion $D'_j$ [120]

$$
\begin{aligned}
N'_j &= N_j + \frac{\tan(\xi)\,\tan(\rho_j)}{c} \\
D'_j &= D_j + \frac{\tan^2(\xi)}{c^2 k_j},
\end{aligned}
\tag{4.6}
$$

where $N_j$ and $D_j$ are the inverse group velocity and inverse group velocity dispersion due to the the material dispersive properties, and $c$ is the speed of light. By performing the second-order Taylor expansion, $\Delta_k$ can be written as a function of the effective inverse group velocities and group velocity dispersion of the all interacting waves

$$
\begin{aligned}
\Delta_k &= (N'_p - N'_s)\Omega_s + (N'_p - N'_i)\Omega_i \\
&+ \frac{1}{2}(D'_p - D'_s)\Omega_s^2 + \frac{1}{2}(D'_p - D'_i)\Omega_i^2 + D'_p \Omega_s \Omega_i,
\end{aligned}
\tag{4.7}
$$

where $\Omega_j$ is the frequency detuning of signal ($j = s$) and idler ($j = i$) photons from the central frequency. The possibility to tune $\Delta_k$, and thereby the frequency correlations, by introducing angular dispersion can be understood by inspecting the effective inverse group velocities $N'_j$ and effective inverse group velocity dispersion $D'_j$ of Eq. (4.6). For the case of type II SPDC processes, where signal and idler wave has different group velocities, we can restrict ourselves only to the first order of Taylor expansion of $\Delta_k$. If signal and idler waves has the same group velocities (type I SPDC process) we have to take into account Taylor expansion of $\Delta_k$ to the second-order.

The joint spectral amplitude $\Phi(\omega_s, \omega_i) \equiv \Phi(\Omega_s, \Omega_i)$ is determined by the spectral shape of the pump beam and by the corresponding effective phase-matching conditions inside the nonlinear crystal. These depend on the relationship between all the group velocities.[14] Under the assumption of type II SPDC process the perfect phase matching is achieved for signal and idler photons angular deviations of angular frequencies that fulfill[105]

$$
\frac{\Omega_i}{\Omega_s} = -\frac{N_p + \frac{\tan(\xi)\tan(\rho_p)}{c} - N_s - \frac{\tan(\xi)\tan(\rho_s)}{c}}{N_p + \frac{\tan(\xi)\tan(\rho_p)}{c} - N_i}.
\tag{4.8}
$$

There are three possible solutions of Eq. (4.8) which corresponds to frequency anticorrelated, correlated and uncorrelated photon pairs. For highly anticorrelated photons in frequency, where $\Omega_s = -\Omega_i$ and effective group velocities are equal

$N_s' = N_i'$, the tilt angle is

$$\xi = \arctan\left(\frac{c(N_i - N_s)}{\tan(\rho_s)}\right). \tag{4.9}$$

For highly frequency correlated photon pairs, $\Omega_s = \Omega_i$, the group velocities fulfills so-called group velocity matching condition[111] $N_p' = (N_s' + N_i')/2$ and the tilt angle is

$$\xi = \arctan\left(\frac{c(2N_p - N_i - N_s)}{\tan(\rho_s) - 2\tan(\rho_p)}\right). \tag{4.10}$$

If we define two spectral intensities $S_{\pm}(\Omega_{\pm}) = \int d\Omega_{\pm}|\Phi(\Omega_+, \Omega_-)|^2$ in the directions $\Omega_{\pm} = \Omega_s \pm \Omega_i$ than frequency anticorrelated (correlated) photons correspond to the case where the bandwidth of $S_+$ is much narrower (wider) than the bandwidth of $S_-$.

The third solution corresponds to frequency uncorrelated photon pairs where ratio between $\Omega_i$ and $\Omega_s$ goes to zero or infinity. There are two possible physical realizations for which the tilt angle can be expressed

$$\xi = \arctan\left(\frac{c(N_p - N_s)}{\tan(\rho_s) - \tan(\rho_p)}\right) \quad \text{or} \quad \xi = \arctan\left(\frac{c(N_i - N_p)}{\tan(\rho_p)}\right). \tag{4.11}$$

## 4.2 Indirect measurement of the frequency correlations

To demonstrate the feasibility of the technique described above we set up an experiment shown in Fig. 4.2.

The second harmonic beam (500 mW of average power, 76 MHz repetition rate) of a femtosecond Ti:Sapphire laser tuned at 810 nm is directed at a diffraction grating $(Gr1)$ that introduces the appropriate amount of pulse-front tilt $(\xi)$ in the plane determined by the pump beam direction of propagation and the optic axis of the nonlinear crystal. The measured bandwidth of the pump beam was $\Delta\lambda_p = 3.6$ nm (FWHM). The pulses diffracted off the grating enter a 2-mm thick BBO crystal where degenerate collinear type-II SPDC occurs. After the downconversion process, the angular dispersion of the downconverted photons is removed by an inverse grating $(Gr2)$.

To evaluate the different types of frequency correlations and the bandwidth, a Hong-Ou-Mandel (HOM) interferometer is used.[9, 105] A variable polarization-dependent delay line made of birefringent quartz (DL) is inserted between the non-linear crystal and the beam splitter, which allows us to add a variable time delay
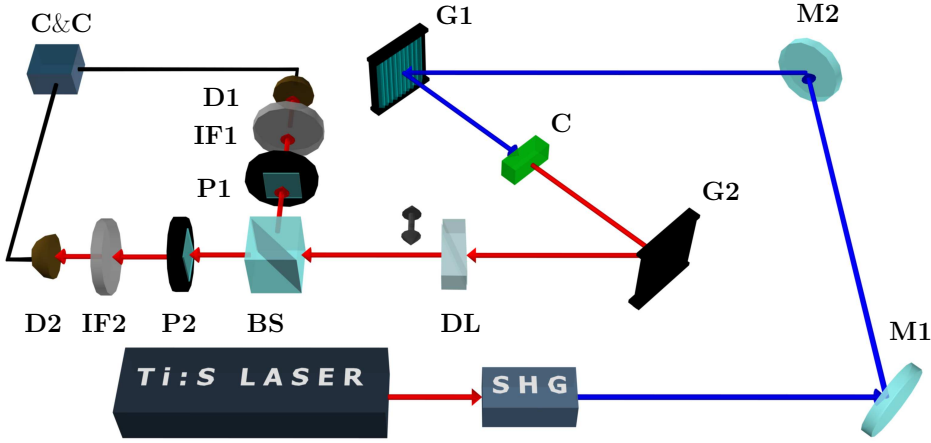
Figure 4.2: Experimental setup. $SHG$: second harmonic generation; $M$: steering mirrors; $Gr$: gratings; $C$ nonlinear crystal; $DL$: delay line; $BS$: beamsplitter; $P$: polarizers; $IF$: 10-nm interference filters; $D$: single-photon avalanche photodiodes; $C\&C$: counter and coincidence electronics.

($\tau$) between the generated paired photons. After the beam splitter, polarizers ($P$) are used to control the polarization of the photons. 10-nm (FWHM) interference filters are located in front of single-photon avalanche photodiodes (SPCM-AQR-14-FC, Perkin-Elmer), where the coincident arrival of two photons in a time window of $\simeq 12$ ns is measured.

The coincidence rate $R\left(\tau, \theta_a = -45^o, \theta_b = 45^o\right)$, where $\theta_{a,b}$ are the angles of the two polarizers, is given by[105,116]

$$R\left(\tau\right) = \frac{1}{2}\left[1 - \frac{1}{2}\int d\Omega_- S_0\left(\Omega_-\right)\exp\left(-i\Omega_-\tau\right)\right], \tag{4.12}$$

where $S_0\left(\Omega_-\right) = \int d\Omega_+ \Phi\left(\Omega_+, \Omega_-\right)\Phi^*\left(\Omega_+, -\Omega_-\right)$.

Fig. 4.3 shows our main experimental results in this section. The normalized number of coincidences (for the sake of comparison) is plotted versus the time delay introduced by the delay line. When no PFT ($\xi = 0^o$) is applied to the pump pulse, the visibility of the HOM dip, defined by Eq. (3.15), drops to $V = 38\%$. The degradation of frequency anticorrelation due to the broadband pump beam introduces distinguishing information between the ordinary and extraordinary downconverted photons. The center of the dip is located at $\tau_0 = \left(N_s' - N_i'\right)L/2$.[121]

The tilt angle for anticorrelated photons is $\xi = 38^o$ and we expect $\tau_0 = 0$. This amount of angular dispersion is introduced by a grating of 1200 lines/mm and diffraction order $m = 1$. Grating $Gr2$ then has 600 lines/mm and $m = -1$. For
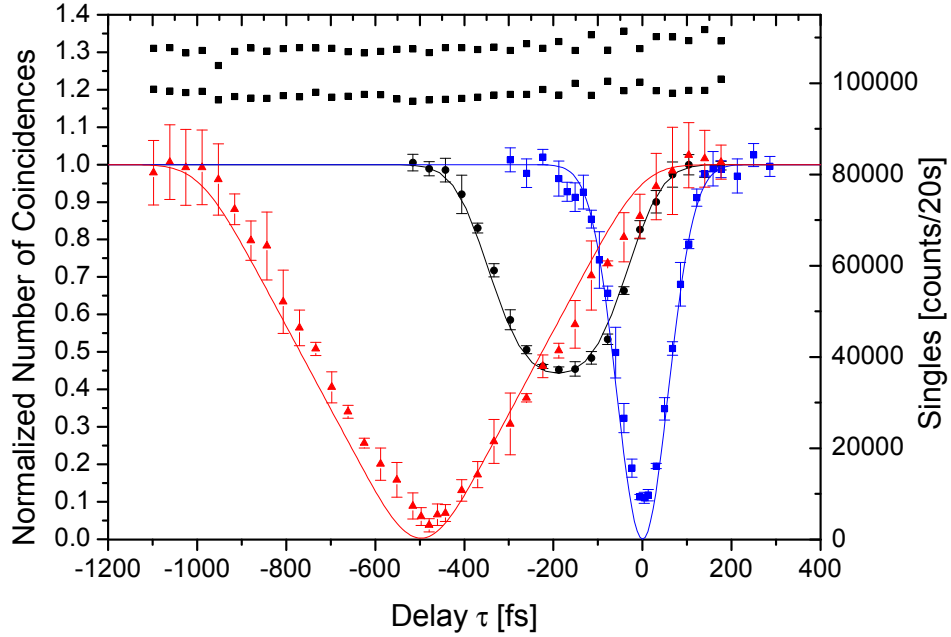
Figure 4.3: Normalized number of coincidences and singles as a function of time delay in a Hong-Ou-Mandel interferometer for three different values of the pulse front tilt of the pump. ●: no pulse-front tilt ($\xi = 0^o$); ■: highly frequency anticorrelated photons ($\xi = 38^o$); ▲: highly frequency correlated photons ($\xi = -52^o$); ■: single counts. Solid lines are the theoretical predictions. The experimental points are raw data without any corrections for measurement noise. The error bars correspond to one standard deviation and are computed from the measured data.

anticorrelated photons we obtain $S_0(\Omega_-) = S_-(\Omega_-)$. The measured visibility of the HOM dip is now 83%. Notice that we generate highly anticorrelated photons even when we are using a broadband pump beam.

The generation of highly correlated photons requires a tilt angle $\xi = -52^o$. We expect $\tau_0 = (N'_s - N'_i)L/2$. A grating Gr1 with 2400 lines/mm and $m = -1$, and Gr2 with 1200 lines/mm and $m = 1$ are used. The spectral intensity writes $S_0(\Omega_-) = S_-(\Omega_-)\exp\{i(N'_s - N'_i)L/2\}$. The visibility of the HOM dip goes up to 93%. The shape of the dip is triangular, as corresponds to a typical type II-like SPDC process.[121] The measured values of $\tau_0$ agree well with the theoretical predictions. Typical values of the measured numbers of coincidences were 6000, 300 and 100 counts/min in the case of no tilt, anticorrelated and correlated photons, respectively. In general, the degree of frequency anticorrelation or correlation might be modified by using crystals of different length or filters with different bandwidth.
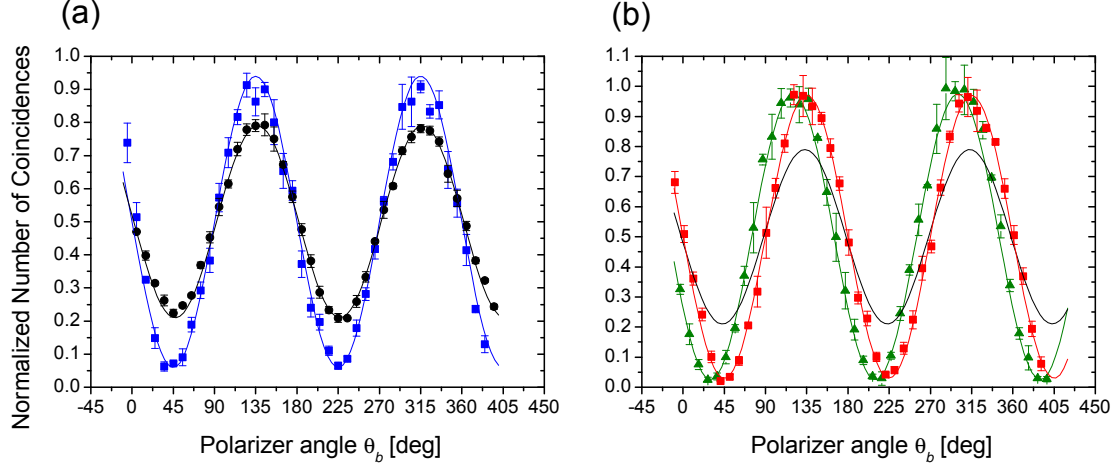
Figure 4.4: Coincidence rate as a function of the polarizer angle $\theta_b$. (a) ■: highly anticorrelated photons. ●: no tilt. (b) ■: highly correlated photons with $\theta_a = -45^o$ and ▲ with $\theta_a = -30^o$; black line: no tilt. Solid lines are $\sin^2$-like fits to the raw experimental data. The error bars correspond to one standard deviation and are computed from the measured data.

The use of frequency correlated (anticorrelated) photons allows the erasing of the distinguishing information coming from the spectra of the photons when considering polarization entanglement. Under our experimental conditions, the two-photon quantum state in polarization space writes

$$|\Psi\rangle\langle\Psi| = \varepsilon|\psi\rangle\langle\psi| + (1-\varepsilon)/2\left\{|H\rangle_s|V\rangle_i\langle H|_s\langle V|_i + |V\rangle_s|H\rangle_i\langle V|_s\langle H|_i\right\}, \quad (4.13)$$

where $|\psi\rangle = 1/\sqrt{2}[|H\rangle_s|V\rangle_i + \exp\{i\Delta\}|V\rangle_s|H\rangle_i]$. The purity of the state is $P = (1 + \varepsilon^2)/2$ and the visibility of $R(\tau_0, \theta_a = -45^o, \theta_b)$ is $V = \varepsilon|\cos\Delta|$.

Fig. 4.4(a) shows $R(\tau_0, \theta_a = -45^o, \theta_b)$ for frequency anticorrelated photons when the angle $\theta_b$ is changed. The corresponding case with no tilt is also shown for comparison. The visibility increases from 58% (no tilt) to 88%. Fig. 4.4(b) shows the case for correlated photons with $\theta_a = -45^o$ and $-30^o$. The visibility goes up to 95% in both cases. Thus the purity of the state is greater than 0.95.

# 4.3 Direct measurement of the frequency correlations

To perform direct measurement of the joint spectral intensity $S(\omega_s, \omega_i)$ we changed previous setup to arrangement depicted in Fig. 4.5. We changed nonlinear crystal to 3.5 mm thick BBO cut for degenerate collinear type-II phase-matching to increase probability of generating photon pairs. Nonlinear crystal was placed between a pair of diffraction gratings: G1 in the path of the pump photons and G2 in the path of the downconverted photons. The first grating introduces the pulse-front tilt and the second grating removes the angular dispersion from the downconverted beam. The crystal was pumped by the second harmonic (220 mW of average power) of a femtosecond Ti:sapphire laser tuned at 800 nm. The measured bandwidth (FWHM) of the pump beam at 400 nm was $\Delta\lambda_p = 2$ nm. After the second grating, the downconverted photons were separated by a polarizing beam splitter (PBS) and collected into multimode fibers. To perform the direct measurement of the joint spectral intensity $S(\omega_s, \omega_i)$, the signal and idler photons were sent to two monochromators (Jobin Yvon MicroHR) Mono1 and Mono2, respectively. The outputs of the monochromators were coupled into optical fibers and detected by single-photon counting modules (SPCM-AQR-14-FC, Perkin-Elmer) in order to record singles and coincidence counts between the two detectors. The joint spectral intensity is measured by scanning the central wavelengths of the bandpass of the monochromators.

The effect of the gratings G1 and G2 is to introduce the appropriate amount of angular dispersion, or equivalently pulse-front tilt $\xi$, into the pulsed pump and the down converted photons. The tilt is introduced in the plane determined by the pump beam and the optic axis of the nonlinear crystal. The gratings were chosen and placed in the setup in such a way that they introduce opposite angular dispersion; this guaranties that the tilt only modifies $\Delta_k$. The groove densities of G1 and G2 were 1200 and 600 grooves per mm, respectively, in the frequency anticorrelated and uncorrelated cases. In the frequency correlated case, the same pair of gratings could have been used, but in order to improve the diffraction efficiency, a pair of gratings with 2400 and 1200 grooves per mm were used instead.

The left column of Fig. 4.6 displays the experimental measurements that demonstrate the full tunability of the frequency correlations of paired photons. The different joint spectral intensities were measured in the same experimental setup at the
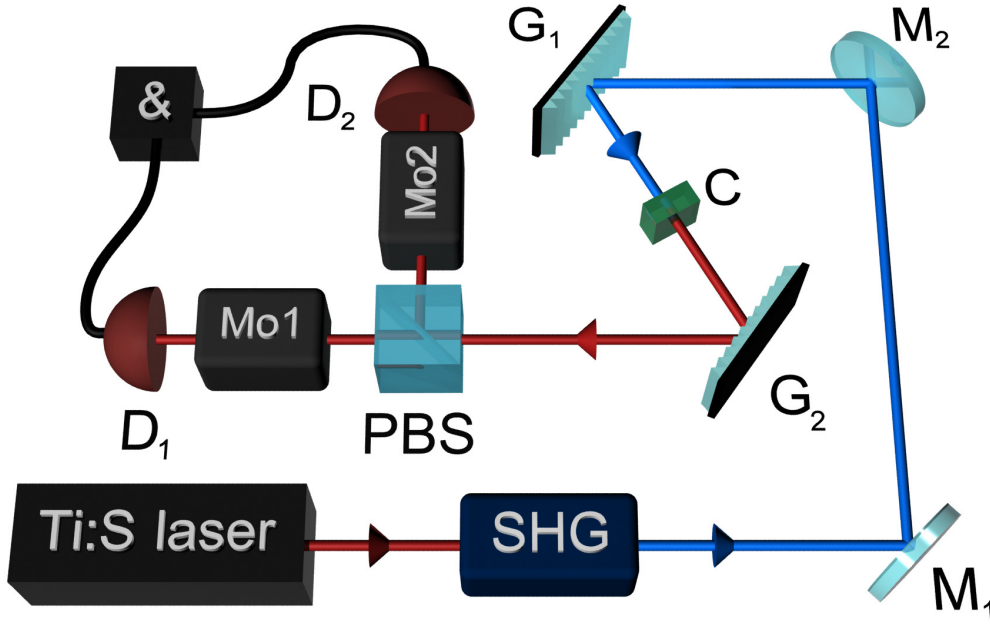
Figure 4.5: Experimental setup. SHG: second harmonic generation; M: dichroic mirrors; G: diffraction gratings; C: nonlinear crystal; PBS: polarization beam splitter. Mono: monochromators. D: single-photon counting modules; &: counter and coincidence electronics.

same pump wavelength and with the same crystal. The only varying parameter was the amount of pulse front tilt $\xi$ introduced by the diffraction gratings. Practically, the tilt tuning was achieved by changing the angle of incidence at the gratings. For the sake of comparison, the theoretical predictions are depicted in the right column. They are obtained by plotting $S\left(\omega_s, \omega_i\right) = |E_p\left(\omega_s + \omega_i\right)|^2 \mathrm{sinc}^2\left(\Delta_k L/2\right)$, where the pump frequency distribution is assumed to be Gaussian with a FWHM bandwidth of $2\,\mathrm{nm}$ and $\Delta_k$ is expanded up to the second order in a Taylor series. The second order, however, introduces only a slight correction as it is the first order that dominates in type II phase matching.

The first row of Fig. 4.6 shows the case with no tilt. As expected for a pulsed pump and type II phase matching, the spectra of the signal and idler are different, one being narrower than the other. This is due to the fact that the downconverted photons have different polarizations and by extension different group velocities and group velocity dispersion. The joint spectrum lies neither along the diagonal $(+45^o)$, nor the antidiagonal line $(-45^o)$. The distinguishability between the spectra of the signal and idler photons results in low visibility in interference experiments with pulsed sources.[111–113]
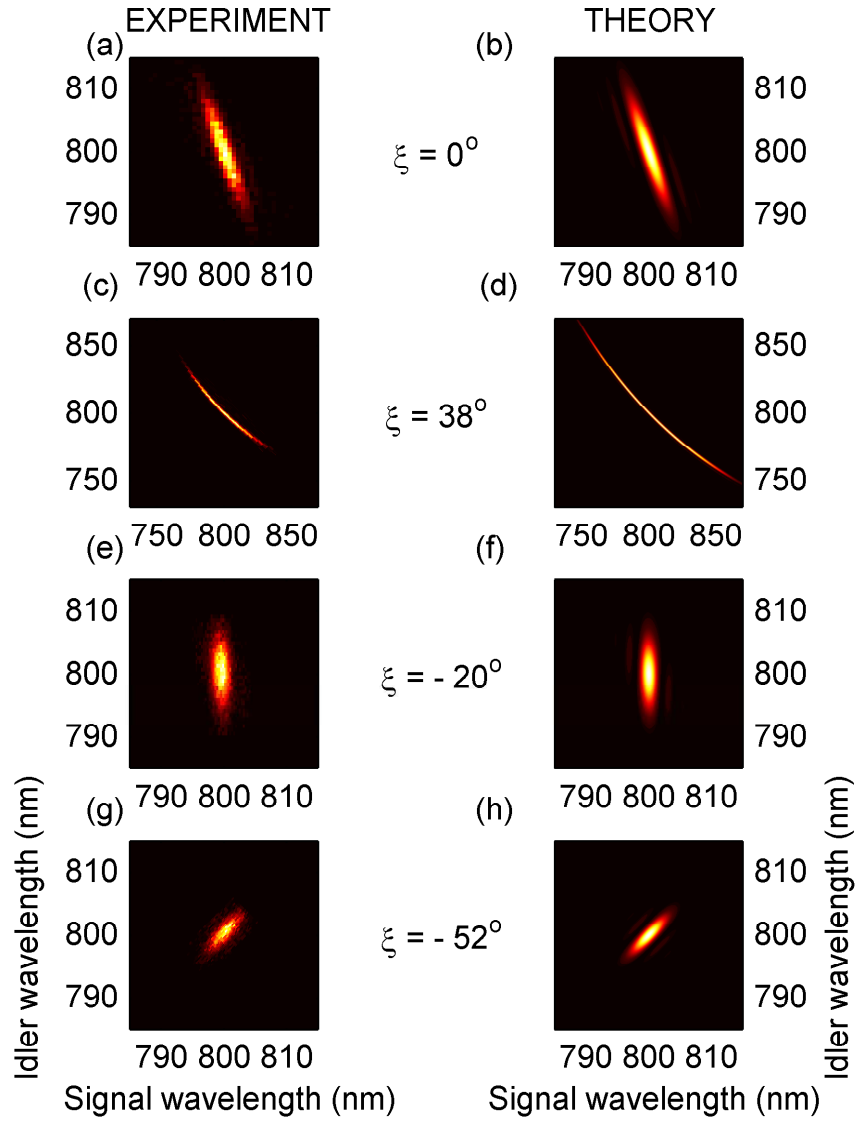
Figure 4.6: Shape of the frequency correlations. Experiment: left column; theoretical prediction: right column. (a) and (b): no tilt, $\xi = 0^o$; (c) and (d): anticorrelated photons, $\xi = 38^o$; (e) and (f): uncorrelated photons, $\xi = -20^o$; (g) and (h): correlated photons $\xi = -52^o$.

The second row of Fig. 4.6 depicts frequency anticorrelated photons, the same type of frequency correlations that would be obtained with a continuous wave pump, but in this case the entangled photon pairs were generated with a broadband pump. The pulse front tilt needed to produce these extremely highly entangled and indistin-

guishable photons was $\xi = 38^o$. The possibility to generate frequency anticorrelated photons with pulsed lasers without the need for filtering is of particular interest in order to obtain high-visibility interference in experiments when the timing information provided by the pump is crucial. This type of frequency correlations exhibit high visibility in a Hong-Ou-Mandel interferometer.[116] The increase in the singles bandwidth to $\sim 90$ nm results in theoretical temporal correlations of the entangled photons of $\sim 12$ fs.[122] Furthermore, the entropy of entanglement is boosted as well, as it is a function of the ratio of the bandwidth of the downconverted photons to the bandwidth of the pump.[122, 123]

The third row of Fig. 4.6 depicts the case of frequency uncorrelated photons $S(\omega_s, \omega_i) = S_s(\omega_s)S_i(\omega_i)$ that was obtained for $\xi = -20^o$. We performed the Schmidt decomposition of the state given by Eq. (4.4) that showed the entropy of entanglement to be nearly $0$.[124] Therefore, the frequency uncorrelation observed in Fig. 4.6 (e) is indeed a signature of the presence of a separable quantum state.

To quantify the degree of frequency uncorrelation of our two-photon state, we fit the experimental data with a Gaussian function of the form $\exp(-a\Omega_s^2 - b\Omega_i^2 - 2c\Omega_s\Omega_i)$.[123] The ratio $c^2/(ab)$ describes its orientation and ellipticity, takes on values between 0 and 1 that correspond to frequency-uncorrelated and maximally entangled states, resp. The obtained value is $c^2/(ab) = 0.01$ with an overlap of the fit and the experimental data of $98.1\%$. Fig. 4.6(e) and (f) show photons with distinguishable spectra. The last row of Fig. 4.6 depicts the direct measurement of photons with frequency correlation. Unlike in work done by O. Kuzucu et al.,[125] where the nonlinear crystal and the wavelength were chosen such as to generate frequency correlated photons, here we obtain the frequency correlation by applying a pulse-front tilt of $\xi = -52^o$ with no need for changing the material, neither the wavelength.

## 4.3.1   Conclusion

Pulses with pulse-front tilt are an important and enabling tool in nonlinear optics, such as in broadband frequency conversion[126, 127] and soliton phenomena in second order nonlinear media.[128, 129] We have shown experimentally that the use of PFT technique allows us tailoring the bandwidth and frequency correlations of entangled photons. The transition from frequency anticorrelated to correlated photons is clearly seen from the experimental data. As cases of particular interest, we have shown the first direct measurement of the joint spectra in which frequency cor-

related photons, and anticorrelated photons were generated using ultrafast pump. We have also demonstrated the generation of frequency uncorrelated photons. In the case of anticorrelated photons, the bandwidth, and thus the entropy of entanglement, were increased resulting in theoretically extremely short temporal correlations. The results reported here are of valuable interest, as the used technique works independently of the wavelength and the nonlinear crystal, and therefore it can be implemented in materials and at wavelengths where conventional solutions do not hold.

PFT techniques can also be used in other configurations. In noncollinear SPDC the group velocity can be tailored too, now with the noncollinear emission angle playing the role of the Poynting-vector walk-off angle. The recently demonstrated generation of paired photons in electromagnetically induced transparency schemes[130] can also benefit from the use of tilted pulses to enhance the control of the frequency correlations of the paired photons, as well as to increase the tuning range of the coherence time of the generated photons.

# Chapter 5

# Experimental realization of programmable quantum gate

Classical computers rely on the combination of a fixed hardware and a flexible software. The operation performed on the data register is fully determined by the information stored in the program register and can be altered at will by the user. It is intriguing to attempt to generalize this concept to quantum computing.[30] Imagine a fixed universal quantum processing unit where the transformation of the data qubits is specified by the quantum state of program qubits. In a seminal paper[77] Nielsen and Chuang proved that an $n$ qubit quantum register can perfectly encode at most $2^n$ distinct quantum operations. Since already unitary transformations on a single qubit form the SU(2) group with uncountably many elements, this bound seems to severely limit the universality of programmable quantum gates.

## 5.1 Quantum gates operation

Although perfect universal programmability is ruled out, it is nevertheless possible to construct approximate programmable quantum gates and optimize their performance for a given size of the program register.[78–83] Two complementary approaches to this problem were pursued in the literature. One option is to design gates that operate deterministically, i.e. always provide an output, but add some noise to the output state.[83] An alternative strategy avoids the extra noise at a cost of reduced success probability.[77–79] The gate then involves a measurement whose outcome heralds its success or failure. If restricted to successful cases, the gate operates perfectly and noiselessly.

A very important elementary programmable quantum gate was proposed by Vidal, Masanes and Cirac (VMC).[78] They considered programmable rotation of a single qubit along the $z$ axis of the Bloch sphere,

$$U(\phi) = |0\rangle\langle 0| + e^{i\phi}|1\rangle\langle 1|. \tag{5.1}$$

Here $|0\rangle$ and $|1\rangle$ denote the computational basis states of the qubit. In the simplest version of VMC protocol, the phase shift $\phi$ is encoded into a state of single-qubit program register,

$$|\phi\rangle_P = \frac{1}{\sqrt{2}}(|0\rangle + e^{i\phi}|1\rangle). \tag{5.2}$$

A C-NOT gate is applied to the data qubit $|\psi\rangle_D = \alpha|0\rangle + \beta|1\rangle$ and the program qubit $|\phi\rangle_P$. This is followed by measurement on the program qubit in the computational basis. The measurement outcome $|0\rangle$ indicates successful application of $U(\phi)$ onto the data qubit while the outcome $|1\rangle$ means that the operation $U(-\phi)$ has been applied. This scheme thus exhibits a success probability of $50\,\%$ which is the maximum possible with a single qubit program register. By adding further program qubits, the probability of success can be made arbitrary close to unity. Note that an exact specification of the phase shift $\phi$ would require infinitely many classical bits. A striking feature of the programmable quantum gate is that the information on $\phi$ is faithfully encoded into *a single* quantum bit.

## 5.2   Quantum gate implementation

While the theory of programmable quantum gates is well established, little attention has been paid to their experimental realizations. The single-qubit programmable quantum measurement devices,[84–93] where the state of program qubit determines the measurement on data qubit, were implemented for single-photons[94] and for nuclear spins in an NMR experiment.[95] Also programmable discriminator of coherent states has been reported.[96,97] However, to our knowledge, there was no demonstration of a programmable unitary quantum gate for photonic qubits, so we have closed this gap between theory and experiment. Specifically, we have implemented the elementary single-qubit programmable gate proposed by VMC.[78]

Our optical implementation is based on the encoding of qubits into polarization states of single photons. We exploit two-photon interference on a polarizing beam splitter (PBS). Consider the input states of data and program photons,

$$|\psi\rangle_D = \alpha|H\rangle + \beta|V\rangle, \qquad |\phi\rangle_P = \frac{1}{\sqrt{2}}(|H\rangle + e^{i\phi}|V\rangle), \tag{5.3}$$

where $|H\rangle$ and $|V\rangle$ denote the horizontal and vertical linear polarization states, respectively. Suppose that the PBS totally transmits horizontally polarized photons and reflects vertically polarized photons. If we restrict ourselves to the cases when a single photon emerges in each output port of the PBS,[131–133] then the conditional two-photon output state reads

$$\frac{1}{\sqrt{2}}(\alpha|H\rangle_D|H\rangle_P + \beta e^{i\phi}|V\rangle_D|V\rangle_P). \tag{5.4}$$

If the program qubit is measured in the diagonal linear polarization basis $|\pm\rangle = \frac{1}{\sqrt{2}}(|H\rangle \pm |V\rangle)$ then the data qubit is prepared according to the measurement result in the state

$$|\psi_{\text{out}}\rangle_D = \alpha|H\rangle \pm \beta e^{i\phi}|V\rangle. \tag{5.5}$$

If the measurement outcome is $|+\rangle$ then the unitary transformation $U(\phi)$ has been applied to the data photon. If the outcome is $|-\rangle$ then the state acquires an extra relative $\pi$ phase shift in the $H/V$ basis. This can be compensated by a fast electrooptical modulator that applies a relative phase shift $0$ or $\pi$ depending on the measurement outcome.[134, 135] With the active feed-forward the scheme achieves the success probability $50\,\%$. This saturates the bound on the achievable success probability[78] so this linear optical scheme is optimal. In the experiment we implemented passive version of the scheme without feed-forward. We post-select only the events when the program qubit is projected onto state $|+\rangle$ which reduces the theoretical success probability of the protocol to $25\,\%$.

## 5.3    Experimental setup

The experimental setup is shown in Fig. 5.1. The initial pump beam from continuous-wave laser (CUBE 405 C, Coherent) with the wavelength of $407\,\text{nm}$ is focused to $6\,\text{mm}$ thick non-linear crystal $\text{LiIO}_3$ cut for type I spontaneous parametric frequency degenerate down-conversion (SPDC). After filtering out the scattered pump light by cut-off filters the down-converted photon pairs with wavelength of $814\,\text{nm}$ are coupled (C) into single-mode optical fibers (SMF) acting as spatial filters. The photons are prepared in horizontal polarization state at the fibers outputs by fiber polarization controllers (PC). To achieve maximal polarization purity two linear film polarizers (P) are employed. The required polarization states of both the data and program photons are set in the preparation stage by properly rotated wave plates $(\frac{\lambda}{2}, \frac{\lambda}{4})$. The data and program photons interfere on the polarizing beam splitter
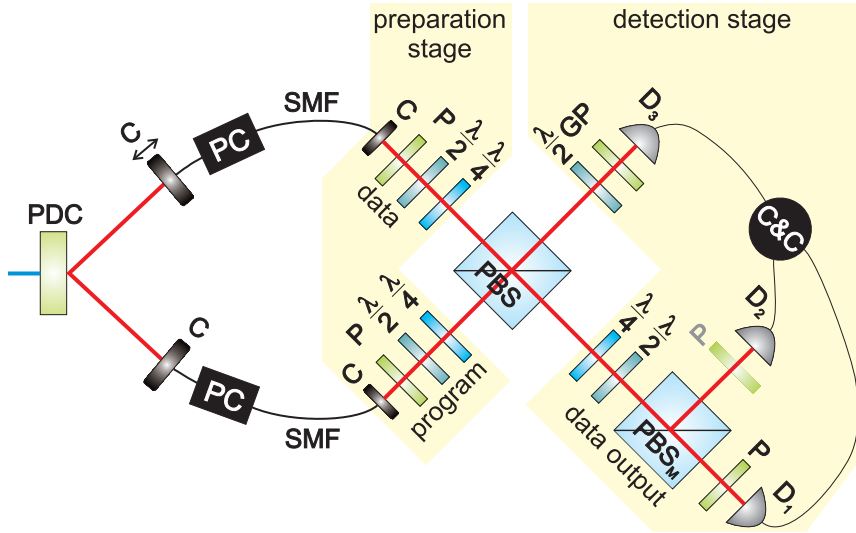
Figure 5.1: Scheme of the experimental setup. The correlated photons generated in the process of spontaneous parametric down-conversion (SPDC) serve as the program and data qubit. After being prepared in proper polarization states the photons interfere on the polarizing beam splitter (PBS). The detection stage consists of polarization analysis, single-photon detectors (D), coincidence logics and counting module (C&C). For polarization setting and analysis the fiber polarization controllers (PC), half-wave plates ($\frac{\lambda}{2}$), quarter-wave plates ($\frac{\lambda}{4}$), polarizers (P), Glan polarizer (GP), and polarization beam splitter (PBS$_M$) are used. See text for details.

(PBS, Ekspla) and enter the detection stage. The data photon passes through a sequence of a quarter-wave plate, a half-wave plate, and another polarizing beam splitter PBS$_M$ which allows to measure the photon in an arbitrary polarization basis. The program photon is projected onto the diagonal linearly polarized state $|+\rangle$ by a half-wave plate and a calcite Glan polarizer (GP). At the outputs the photons are detected by fiber-coupled single-photon avalanche photodiodes (SPCM-AQ4C, Perkin Elmer). Detection events registered by the detectors $D_1$, $D_2$, and $D_3$ are processed by coincidence logic (TAC/SCA, Ortec) and fed into a counting module (Ortec).
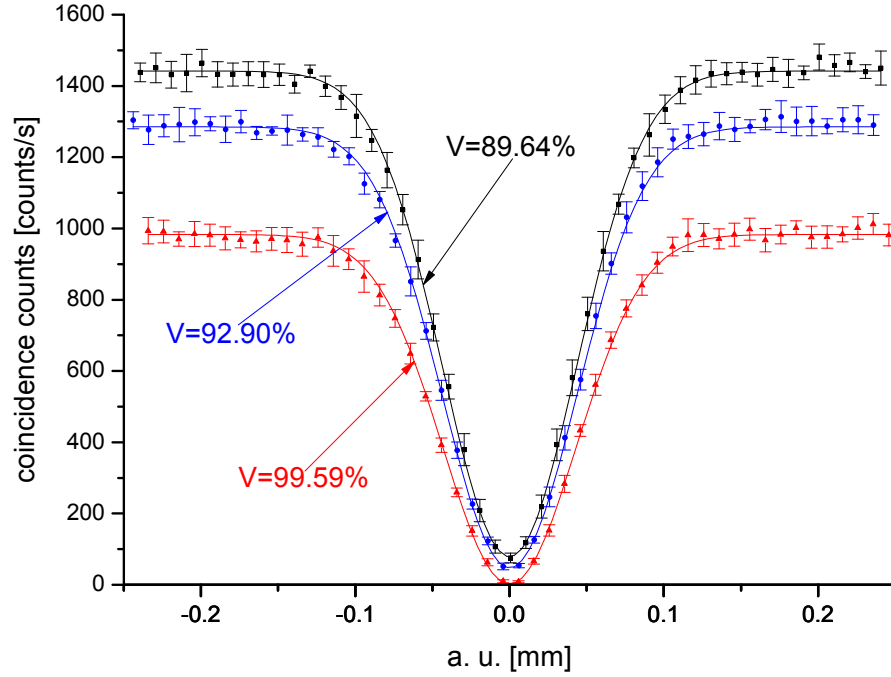
Figure 5.2: The measured HOM dip visibility of correlated photon pairs on $PBS_M$ without linear film polarizers (■), with linear film polarizer placed in front of APD $D_1$ (•) and with linear film polarizers placed in front of APDs $D_1$ and $D_2$ (▲). The error bars correspond to one standard deviation and are computed from the measured data.

## 5.4    Spatial mode functions overlap on the PBS

To verify the overlap of photons' spatial mode functions on the PBS we measure the visibility of Hong-Ou-Mandel (HOM) dip[9] in the data output port. The data and program photons are prepared in horizontal and vertical polarization states, respectively, so that they both propagate to the data output. The wave plates in the data detection stage are set to transform the H/V linear polarizations onto the diagonal ones. The HOM dip in coincidences between clicks of detectors $D_1$ and $D_2$ is measured as a function of the time delay between the program and data photons introduced by a motorized translation of one of the fiber coupling systems. The measured HOM dip visibility is above 89 %, limited mainly by imperfections of $PBS_M$. Particularly, if we insert two linear film polarizers in front of APDs $D_1$ and $D_2$ the visibility exceeds 99.5 %, see Fig. 5.2. This indicates nearly perfect spatial overlap of the data and program photons on PBS. The linear film polarizer placed before detector $D_2$ is removed in further measurements and used in the state

preparation stage to ensure preparation of pure input state.

## 5.5    Measurement

The success of the gate is heralded by a coincidence detection of a single photon in each output port. In the experiment, we therefore measure the coincidence rates $C_{13}$ between detectors $D_1$ and $D_3$ and $C_{23}$ between detectors $D_2$ and $D_3$. The width of the coincidence window is set to 2 ns. For a given phase shift $\phi$ we characterize the performance of the programmable gate by a tomographically complete measurement. We set the state of the program photon to $\frac{1}{\sqrt{2}}(|H\rangle + e^{i\phi}|V\rangle)$. We then subsequently prepare the data photon in six different states $|H\rangle$, $|V\rangle$, $|+\rangle$, $|-\rangle$, $|R\rangle$ and $|L\rangle$, where $|R\rangle = \frac{1}{\sqrt{2}}(|H\rangle + i|V\rangle)$ and $|L\rangle = \frac{1}{\sqrt{2}}(|H\rangle - i|V\rangle)$ denote the right and left circularly polarized states, respectively. For each input we carry out measurements for six different settings of the wave plates in the data detection stage chosen such that the click of $D_1$ heralds projection of the data photon onto the state $|H\rangle$, $|V\rangle$, $|+\rangle$, $|-\rangle$, $|R\rangle$, and $|L\rangle$ by turns. Every particular measurement takes 5 s and is repeated 10 times to gain statistics. Average twofold coincidence rate is about 1300 s$^{-1}$. The polarizer placed in front of the detector $D_1$ guarantees nearly ideal projection onto a pure polarization state. Therefore, the presented results were obtained using only $C_{13}$ coincidence data. Note that in this way we do not need to precisely calibrate the relative detection efficiencies of $D_1$ and $D_2$. We have confirmed that the results remain largely unchanged if we use the coincidences $C_{23}$ instead or if we process all data simultaneously. However, the results obtained from $C_{23}$ exhibit slightly higher noise due to imperfect polarization filtering by the polarizing beam splitter PBS$_M$. The process and state fidelities determined using coincidences $C_{23}$ are about 1 % lower than the fidelities obtained from coincidences $C_{13}$.

## 5.6    Data analysis

From the experimental data we reconstruct the completely positive (CP) map that fully characterizes the transformation of the data photon for a fixed state of the program photon. We have performed the quantum process tomography for eight different phase shifts $\phi = \frac{k}{4}\pi$, $k = 0, 1, ..., 7$. According to the Jamiolkowski-Choi isomorphism,[136, 137] every CP map can be represented by a positive semidefinite op-

erator $\chi$ on the tensor product of the input and output Hilbert spaces $\mathcal{H}_\text{in}$ and $\mathcal{H}_\text{out}$. In our case both $\mathcal{H}_\text{in}$ and $\mathcal{H}_\text{out}$ are two-dimensional Hilbert spaces of polarization state of a single photon hence $\chi$ is a $4 \times 4$ matrix. The input state $\rho_\text{in}$ transforms according to the formula $\rho_\text{out} = \text{Tr}_\text{in}[(\rho_\text{in}^T \otimes 1_\text{out})\,\chi]$, where $T$ denotes transposition in a fixed basis. Due to the slight imperfections of the PBS, the implemented operation is not exactly unitary and may involve some polarization filtering. We therefore do not impose the constraint that $\chi$ has to be trace-preserving but allow for general trace-decreasing map.[138, 139] We use the iterative maximum-likelihood estimation algorithm that is described in detail elsewhere.[140, 141] This nonlinear statistical reconstruction method yields a quantum process $\chi$ that is most likely to produce the observed experimental data.[142, 143]

Fig. 5.3 displays the real and imaginary parts of the reconstructed CP map $\chi$ for four different phase shifts $\phi = k\frac{\pi}{2}$, $k = 0, 1, 2, 3$. We quantify the gate performance by the process fidelity defined as follows,

$$F_\chi = \frac{\text{Tr}[\chi\chi_\text{id}(\phi)]}{\text{Tr}[\chi]\text{Tr}[\chi_\text{id}(\phi)]}. \tag{5.6}$$

Here $\chi_\text{id}(\phi)$ is a process matrix representing the unitary operation $U(\phi)$ (5.1),

$$\chi_\text{id}(\phi) = 1 \otimes U(\phi)|\Phi^+\rangle\langle\Phi^+|1 \otimes U^\dagger(\phi), \tag{5.7}$$

where $|\Phi^+\rangle = |H\rangle|H\rangle + |V\rangle|V\rangle$ denotes the maximally entangled Bell state. Thus $\chi_\text{id}$ is effectively a density matrix of a pure maximally entangled state on $\mathcal{H}_\text{in} \otimes \mathcal{H}_\text{out}$. The process fidelity determined from the reconstructed CP maps is plotted in Fig. 5.4 as a function of the phase shift $\phi$. We can see that the fidelity is almost constant and exceeds $95\,\%$ for all values of $\phi$ which demonstrates very good functionality of the programmable gate.

A careful analysis of the reconstructed CP maps reveals that the polarizing beam splitter PBS imposes certain non-zero relative phase shift $\delta\phi$ between the vertical and horizontal polarizations. The active area of the PBS where splitting of the vertical and horizontal polarization components occurs is made of a stack of thin dielectric films. In principle, each of the polarization and spatial modes passing through the PBS can acquire a different phase shift. However, only a single effective combination of such phase shifts is relevant in our experiment and gives rise to the phase offset $\delta\phi$.

We estimate the phase offset as follows. For each value of the encoded phase shift $\phi$ we determine the effective applied phase shift $\phi_\text{eff}$ by maximizing the overlap $\text{Tr}[\chi\chi_\text{id}(\phi_\text{eff})]$ over $\phi_\text{eff}$. The dependence of $\phi_\text{eff}$ on $\phi$ is plotted in Fig. 5.5.
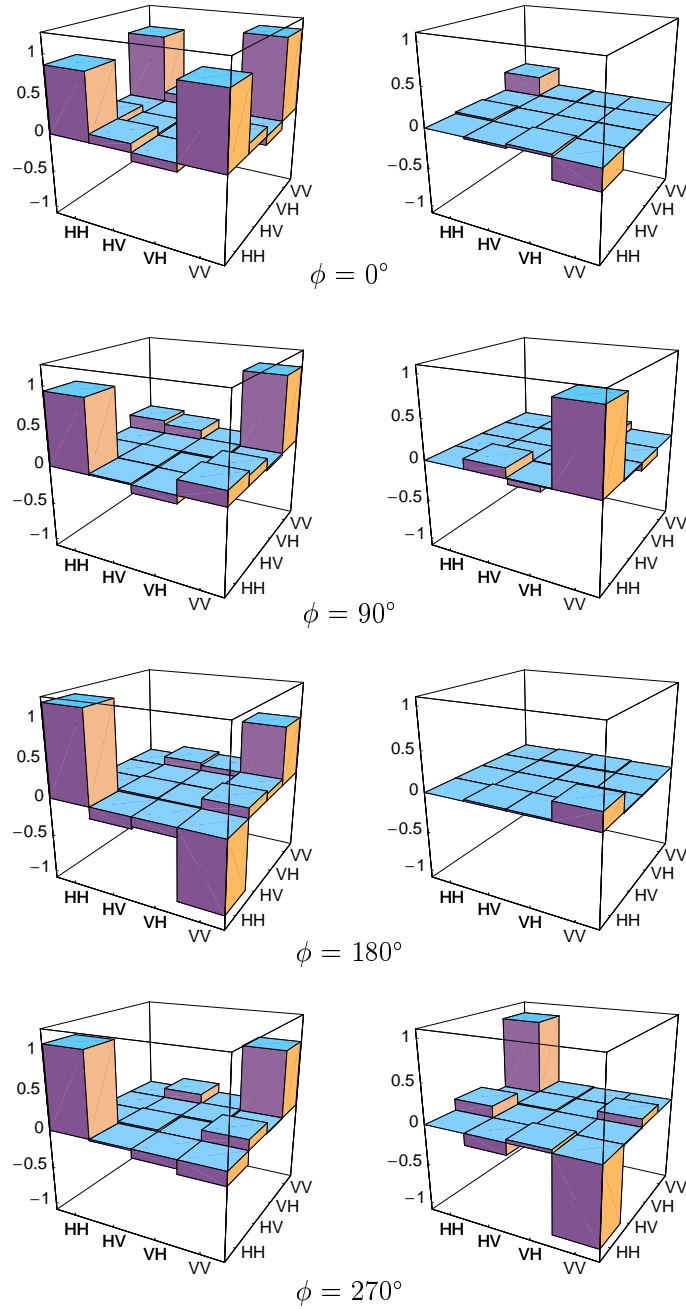
Figure 5.3: Reconstructed process matrix $\chi$. Real (left column) and imaginary (right column) parts of the reconstructed CP map $\chi$ are shown for four different values of the programmed phase shift $\phi$ encoded in the state of program photon.

From the best linear fit to the data we obtain $\delta\phi = -0.265\,\text{rad}$. This phase offset could be passively compensated e.g. by means of additional wave-plates that would apply the relative phase shift $-\delta\phi$ to the output data photon. We have carried
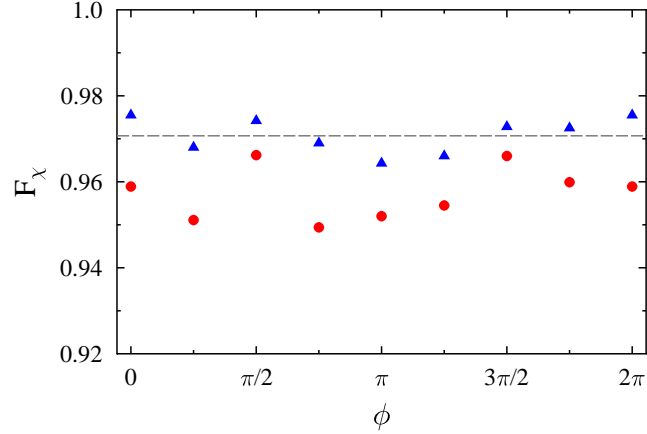
Figure 5.4: Quantum process fidelity of the programmable gate is plotted as a function of the encoded phase shift $\phi$. The fidelities before ($\bullet$) and after ($\blacktriangle$) compensation of the constant phase offset $\delta\phi$ are shown. The dashed line represents the best constant fit to the compensated fidelity data with the value of 97.1 %.

out the software compensation and corrected the reconstructed CP maps for the fixed phase offset. This calibration procedure increases the process fidelity by about 1 % as shown in Fig. 5.4. All the compensated fidelity data are within one percent around the average value of 97.1 %. The achievable gate fidelity is mainly limited by the imperfections of the polarizing beam splitter PBS that does not totally reflect (transmit) the V (H) polarization. The measured splitting ratios read 98 : 2 and 0.5 : 99.5 for horizontal and vertical polarizations, respectively. A simple theoretical model predicts average process fidelity 97.7 % which is in a very good agreement with the experimental results.

Besides the quantum processes we have also reconstructed the single-qubit output state for each input state. We have evaluated the state fidelity $F = \langle\psi_{\mathrm{out}}|\rho|\psi_{\mathrm{out}}\rangle$ between the expected pure output state and the reconstructed (generally mixed) state $\rho$. For each phase shift $\phi$ we average the state fidelity over the six different input states to obtain the average state fidelity $F_{\mathrm{avg}}$. We find that $F_{\mathrm{avg}}$ lies in the interval 96.6 % − 97.8 %. The compensation of the phase offset $\delta\phi$ increases the average state fidelity by almost 1 % to the range 97.6 % − 98.5 %. This further confirms that the programmable gate operates with very high fidelity for all values of the phase shift $\phi$ in the interval $[0, 2\pi]$.

The average state fidelity $F_{\mathrm{avg}}$ and the process fidelity $F_\chi$ exhibit almost perfect linear dependence of the form $F_{\mathrm{avg}} = 0.727F_\chi + 0.275$. This is consistent with
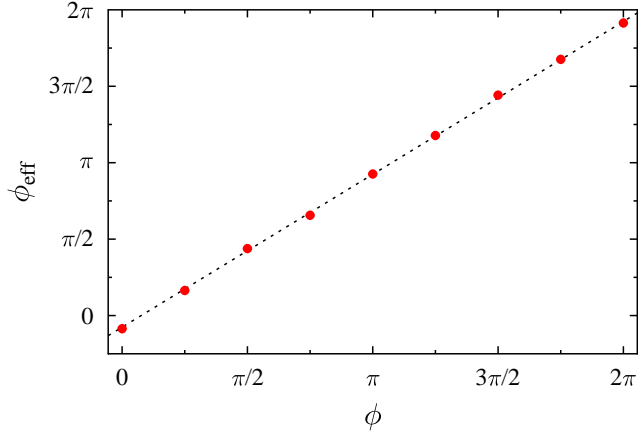
Figure 5.5: Dependence of the effectively applied phase shift $\phi_{\text{eff}}$ on the programmed phase shift $\phi$. The circles represent results obtained from 8 reconstructed CP maps, the dashed line is the best linear fit to the data.

the theoretically predicted relation between these two fidelities for deterministic processes,[144] $F_{\text{avg}} = \frac{1}{3}(2F_\chi + 1)$. The observed discrepancy is mainly due to the fact that we perform independent maximum likelihood reconstructions of the quantum process and output states while the theoretical formula assumes that the output states are calculated from the input states using the process matrix $\chi$. Also, the reconstructed CP map is not exactly trace preserving.

## 5.7    Other application of the realized quantum gate

We next show that our device can also function as a programmable partial polarization filter.[81] For this purpose we prepare the program qubit in various linear polarization states $\cos\theta|H\rangle + \sin\theta|V\rangle$. Repeating the calculation leading to Eq. (5.5) we find the (non-normalized) output state of the data qubit to be

$$|\psi_{\text{out}}\rangle_T = \alpha\cos\theta|H\rangle + \beta\sin\theta|V\rangle. \tag{5.8}$$

The amplitude of vertical polarization is attenuated (or amplified) by a factor of $\tan\theta$ with respect to amplitude of the horizontal polarization. We carry out the complete quantum process tomography of the programmable quantum filter for nine different values of $\theta = \frac{n}{16}\pi$, $n = 0, 1, ..., 8$. The process fidelity can be calculated according to Eq. (5.6) where the ideal filtering operation is now described by a partially entangled state, $\chi_{\text{id,filter}}(\theta) = (\cos\theta|H\rangle|H\rangle + \sin\theta|V\rangle|V\rangle)(\langle H|\langle H|\cos\theta +$
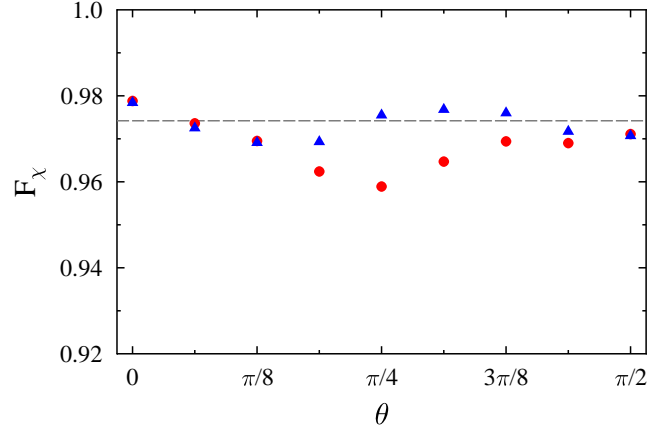
Figure 5.6: Quantum process fidelity of the programmable partial polarization filter is plotted as a function of the filtering angle $\theta$. The fidelities before ($\bullet$) and after ($\blacktriangle$) compensation of the constant phase offset $\delta\phi$ are shown. The dashed line represents the best constant fit to the compensated fidelity data with the value of 97.4%.

$\langle V|\langle V|\sin\theta)$. The experimentally determined process fidelity is plotted in Fig. 5.6. Similarly as for the programmable unitary gate, the compensation of the constant phase offset $\delta\phi$ increases the fidelity. The improvement is most significant for $\theta = \pi/4$ while for complete filtering ($\theta = 0$ and $\theta = \pi/2$) the phase shift is irrelevant and its compensation does not change the fidelity.

## 5.8 Conclusion

The programmable single-qubit phase gate working on single-photon polarization-encoded qubits has been proposed and experimentally developed. The gate operation has been thoroughly tested by complete quantum process tomography. The comparison of the reconstructed processes and the corresponding theoretical ones yields high process fidelity of about 97 % with negligible dependence on the encoded phase shift. It was demonstrated that with a different set of program states, the device can also operate as a programmable partial polarization filter. The implemented programmable gates can serve as building blocks of more complex multi-qubit linear-optics quantum gates or other optical quantum information processing devices.

# Chapter 6

# Optimal two-copy discrimination of quantum measurements

Two non-orthogonal quantum states cannot be perfectly distinguished. This fundamental constraint has important practical consequences as it for instance guarantees the security of certain quantum key distribution protocols. Even if perfect discrimination is ruled out, one can nevertheless try to perform this task in an approximate manner. Various strategies for optimal approximate discrimination of quantum states have been studied since the seminal work of Holevo[145] and Helstrom.[146] The rapid development of quantum information theory during recent years stimulated investigation of discrimination of more complex quantum objects, namely quantum operations, channels, and measurements.[147–157] The role of entanglement in discrimination of quantum operations and channels has been studied in some detail[158–163] and experimental realizations of several discrimination schemes for quantum operations have been reported.[164, 165] Very recently, quantum combs have been established as a general framework for treating the problems of discrimination and cloning of quantum operations.[166, 167]

Although formally the discrimination of quantum states and operations may look quite similar at first glance, there are important differences due to the richer inherent structure of quantum operations. For instance, any two different unitary operations $U$ and $V$ can be perfectly and deterministically discriminated provided that a sufficient finite number of applications of the operation is accessible.[148] Similarly, perfect discrimination between two different projective quantum measurements is possible with finite number of uses of the measuring apparatus.[152] In contrast, two non-orthogonal quantum states cannot be perfectly deterministically discriminated from an arbitrary finite number of copies.

In the present chapter, we shall investigate in detail various strategies for discrimination among two quantum measurements.[152–154] We shall assume that we are given a measuring apparatus $M$ that performs one of two single-qubit projective measurements $A$ or $B$. Our goal is to determine as well as possible whether $M = A$ or $M = B$ for a given fixed finite number of allowed utilizations of the measuring apparatus $M$. In particular, we shall focus on the scenario where the measurement $M$ can be performed twice. We will refer to this scenario as two-copy discrimination of quantum measurements. We will assume that no further auxiliary measurements could be performed on some ancilla states, so the identity of the measurement has to be determined solely from the two outcomes of $M$. Already within this setting there exist several different discrimination strategies of varying complexity and performance. We will show that adaptive discrimination, entangled probe states, and feed-forward all help to enhance the probability of correct identification of the measurement. By combining entangled probes and feed-forward, perfect deterministic discrimination of projective measurements is possible provided that their distance is sufficiently large.[152] Here we explicitly derive the entangled probe state and feed-forward operation that enable perfect two-copy discrimination for a large class of pairs of single-qubit measurements. We also show a successful proof-of-principle experimental realization of the studied discrimination strategies.

## 6.1   Discrimination strategies

Throughout the chapter, the two single-qubit projective measurements that should be discriminated will be labeled by letters $A$ and $B$. The two possible measurement outcomes will be denoted as 0 and 1, respectively. Without loss of any generality we can choose the two projective measurements in the following form,

$$
\begin{aligned}
\Pi_{A,0} &= |0\rangle\langle 0|, \qquad \Pi_{B,0} = |\theta\rangle\langle\theta|, \\
\Pi_{A,1} &= |1\rangle\langle 1|, \qquad \Pi_{B,1} = |\theta_\perp\rangle\langle\theta_\perp|,
\end{aligned}
\tag{6.1}
$$

where

$$
|\theta\rangle = \cos\theta|0\rangle + \sin\theta|1\rangle, \quad |\theta_\perp\rangle = \sin\theta|0\rangle - \cos\theta|1\rangle.
\tag{6.2}
$$

The angle $\theta \in [0, \pi/2]$ parameterizes the overlap $\mathcal{O}$ between the two measurements that can be naturally defined as

$$
\mathcal{O} = \mathrm{Tr}[\Pi_{A,0}\Pi_{B,0}] = \mathrm{Tr}[\Pi_{A,1}\Pi_{B,1}] = \cos^2\theta.
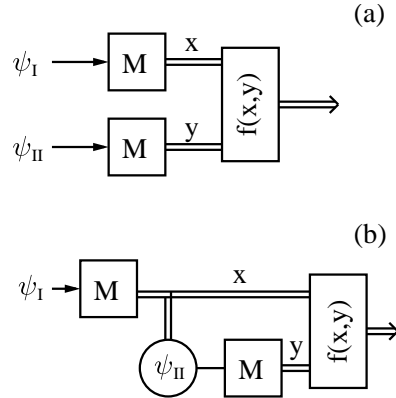\tag{6.3}
$$

Figure 6.1: Discrimination of single-qubit quantum measurements with single-qubit probe states. In the considered scenario the measurement $M$ can be performed twice. (a) Discrimination using two fixed probe states $|\psi_\mathrm{I}\rangle$ and $|\psi_\mathrm{II}\rangle$. (b) Adaptive discrimination strategy where the second probe state $|\psi_\mathrm{II}\rangle$ is chosen according to the result of the first measurement $x$. Time flows from the left to the right. Single lines indicate quantum bits, double lines classical bits.

We shall assume that the *a-priori* probability of each measurement is $\frac{1}{2}$ and that no other auxiliary measurements could be performed. Although interesting phenomena arise mainly when several uses of the measurement are allowed, let us for the sake of completeness first consider the situation when the measurement can be performed only once. A single-qubit probe state $|\psi\rangle$ is sent to the measuring apparatus and if the measurement outcome reads 0 (1) then we guess that the measurement $A$ ($B$) was performed. The probability of correct guess $P_\mathrm{succ}$ is maximized if $|\psi\rangle$ is chosen as the eigenstate corresponding to the largest eigenvalue of operator $\Pi_{A,0} + \Pi_{B,1}$. We obtain

$$|\psi\rangle = \frac{1}{\sqrt{2(1 - \sin\theta)}} \left(\cos\theta|0\rangle + (\sin\theta - 1)|1\rangle\right), \qquad (6.4)$$

and

$$P_\mathrm{succ} = \frac{1}{2}(1 + \sin\theta). \qquad (6.5)$$

Let us now assume that the measurement can be performed twice. In this case we can distinguish four different discrimination strategies, as illustrated in Figs. 6.1 and 6.2. The most straightforward approach is the probing by two fixed single-qubit states, see Fig. 6.1(a). The measurement is then inferred from the two measurement results $x, y \in \{0, 1\}$. The discrimination strategy is formally described
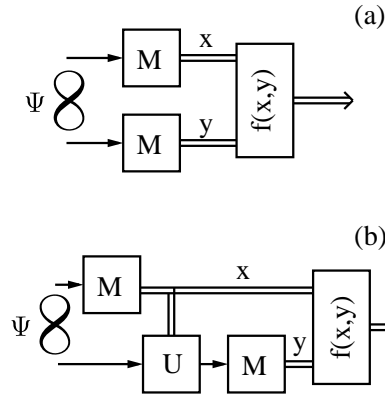
Figure 6.2: (a) Discrimination of quantum measurements using entangled probe state $|\Psi\rangle$. (b) Feed-forward enhanced discrimination of quantum measurements. A unitary operation $U$ depending on the measurement outcome $x$ on the first part of the entangled state is applied to the second part of the entangled state prior to the measurement.

by a function $f(x,y)$ that assigns an estimate A or B to each of the four possible pairs of outcomes 00, 01, 10, 11. There are altogether $2^4 = 16$ such functions and when determining the optimal discrimination strategy, we must optimize over all those 16 alternatives.

The strategy shown in Fig. 6.1(a) can be improved by using an adaptive scheme, where the second single-qubit probe state $|\psi_{\mathrm{II}}\rangle$ becomes dependent on the outcome $x$ of the measurement on the first probe state $|\psi_{\mathrm{I}}\rangle$, cf. Fig. 6.1(b). There are thus two different second probe states $|\psi_{\mathrm{II},0}\rangle$ and $|\psi_{\mathrm{II},1}\rangle$ that can be optimized independently. As we shall show below, this adaptive procedure increases the probability of successful guess of the correct measurement.

So far we have considered probing by single-qubit states. A more general strategy, however, could explore an entangled two-qubit state as a probe, as illustrated in Fig. 6.2(a). Moreover, we can combine the entanglement with feed-forward and after performing the measurement on the first qubit of the entangled state we can apply to the second qubit a unitary operation $U(x)$ that depends on the outcome of the first measurement.[152] This most advanced discrimination strategy is depicted in Fig. 6.2(b). This latter approach allows for perfect deterministic two-copy discrimination provided that $\theta \geq \frac{\pi}{4}$.

## 6.2 Probing with separable states

Let us first concentrate on the probing with two pure fixed single-qubit states as shown in Fig. 6.1(a). We choose as a figure of merit that should be maximized the probability of successful guess of the measurement,

$$P_{\text{succ}} = \frac{1}{2} \sum_{x=0}^{1} \sum_{y=0}^{1} \text{Tr}[\psi_{\text{I}}\Pi_{f(x,y),x}]\text{Tr}[\psi_{\text{II}}\Pi_{f(x,y),y}]. \tag{6.6}$$

Here $\psi_j = |\psi_j\rangle\langle\psi_j|$ is a short-hand notation for a density matrix of a pure state. Because of convexity, the pure probe states are always optimal as can be directly seen from the structure of the formula (6.6). For a fixed $\psi_{\text{I}}$ and $f(x,y)$ the optimal $\psi_{\text{II}}$ can be determined as the eigenstate of the operator

$$R = \frac{1}{2} \sum_{x=0}^{1} \sum_{y=0}^{1} \text{Tr}[\psi_{\text{I}}\Pi_{f(x,y),x}]\Pi_{f(x,y),y} \tag{6.7}$$

that corresponds to the maximum eigenvalue $r_{\text{max}}$ of $R$. Maximizing $r_{\text{max}}$ over all 16 functions $f(x,y)$ and over all probe states $\psi_{\text{I}}$ then yields $P_{\text{succ}}$. We have performed this optimization numerically and found that the optimal $f(x,y)$ is asymmetric, guess A is made for three outcomes and guess B is made only for one outcome,

$$f(0,0) = A, \quad f(0,1) = A, \quad f(1,0) = A, \quad f(1,1) = B. \tag{6.8}$$

Moreover, the optimal $\psi_{\text{I}}$ and $\psi_{\text{II}}$ lie in the same plane of the Bloch sphere as the projectors (6.1), which is intuitively plausible. We can thus write

$$\begin{aligned} |\psi_{\text{I}}\rangle &= \cos\phi_I|0\rangle + \sin\phi_I|1\rangle, \\ |\psi_{\text{II}}\rangle &= \cos\phi_{\text{II}}|0\rangle + \sin\phi_{\text{II}}|1\rangle. \end{aligned} \tag{6.9}$$

Assuming the form (6.9) of $\psi_{\text{I}}$ and the guessing prescription (6.8), the whole optimization can be performed analytically. After some algebra one arrives at the expression for the optimal angle $\phi_I$,

$$\phi_{\text{I}} = \frac{1}{2}\left(\theta - \arccos\left[\frac{1}{4\cos\theta}\left(1 - \sqrt{1 + 8\cos^2\theta}\right)\right]\right). \tag{6.10}$$

The corresponding success probability reads

$$\begin{aligned} P_{\text{succ,sep}} &= \frac{1}{2} + \frac{\tan\theta}{8\sqrt{2}}\sqrt{1 + 2\cos(2\theta) + \sqrt{5 + 4\cos(2\theta)}} \\ &\quad + \frac{\sin\theta}{4\sqrt{2}}\sqrt{2 + \cos(2\theta) + \sqrt{5 + 4\cos(2\theta)}}. \end{aligned}$$

$$\tag{6.11}$$

Furthermore, it holds that it is optimal to set $\phi_{\text{II}} = \phi_{\text{I}}$, hence the two optimal probe states $\psi_{\text{I}}$ and $\psi_{\text{II}}$ are in fact identical.

Let us now move to the second scenario, where the second probe state $\psi_{\text{II}}$ is chosen according to the result $x$ of the first measurement. The success probability of this protocol can be expressed as

$$P_{\text{succ}} = \frac{1}{2} \sum_{x=0}^{1} \sum_{y=0}^{1} \text{Tr}[\psi_{\text{I}} \Pi_{f(x,y),x}] \text{Tr}[\psi_{\text{II},x} \Pi_{f(x,y),y}]. \tag{6.12}$$

For each $f(x,y)$ and $\psi_{\text{I}}$ the two probe states $\psi_{\text{II},0}$ and $\psi_{\text{II},1}$ have to be optimized independently. They can be determined as eigenstates corresponding to maximum eigenvalues $r_{\text{max},0}$ and $r_{\text{max},1}$ of operators

$$R_0 = \sum_{y=0}^{1} \text{Tr}[\psi_{\text{I}} \Pi_{f(0,y),0}] \Pi_{f(0,y),y},$$

$$R_1 = \sum_{y=0}^{1} \text{Tr}[\psi_{\text{I}} \Pi_{f(1,y),1}] \Pi_{f(1,y),y}. \tag{6.13}$$

The optimal discrimination strategy can be determined by maximizing $r_{\text{max},0} + r_{\text{max},1}$ over all $f(x,y)$ and $\psi_{\text{I}}$. Numerical maximization reveals that, again, optimal $\psi$ all lie in the same plane as projectors (6.1) and are thus of the form (6.9). The optimal function $f(x,y)$ is now symmetric,

$$f(0,0) = A, \quad f(0,1) = B, \quad f(1,0) = A, \quad f(1,1) = B. \tag{6.14}$$

The optimization of the angles $\phi_{\text{I}}$, $\phi_{\text{II},0}$ and $\phi_{\text{II},1}$ can be again performed fully analytically and we obtain

$$\phi_{\text{I}} = \frac{\pi}{4} + \frac{\theta}{2}. \tag{6.15}$$

The explicit formulas for the angles $\phi_{\text{II},0}$ and $\phi_{\text{II},1}$ are rather unwieldy and are not reproduced here. Instead, we plot the dependence of the optimal $\phi_j$ on $\theta$ in Fig. 6.3. Note that generally $\phi_{\text{II},0} \neq \phi_{\text{II},1}$ which is a signature of the adaptive discrimination strategy. The maximum achievable probability of success reads

$$P_{\text{succ,ad}} = \frac{1}{2} \left( 1 + \sqrt{1 - \cos^4 \theta} \right). \tag{6.16}$$

It can be explicitly checked that for all $\theta \in (0, \pi/2)$ it holds that $P_{\text{succ,ad}} > P_{\text{succ,sep}}$ so the adaptive strategy strictly outperforms the strategy where the probe single-qubit states are a-priori fixed.
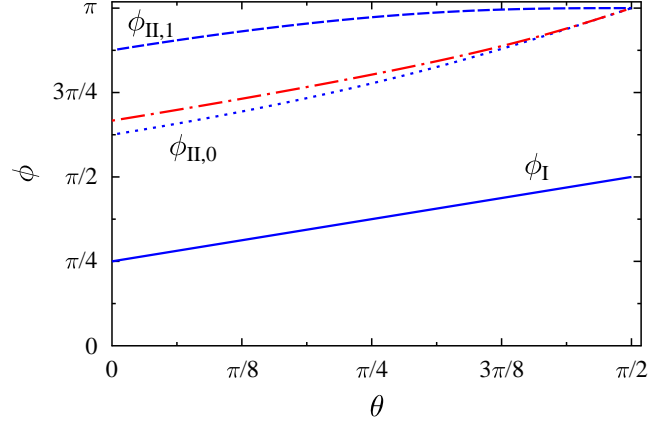
Figure 6.3: The angles $\phi_j$ parameterizing optimal probe single-qubit states are plotted in dependence on $\theta$. Shown are the optimal angles for adaptive strategy $\phi_\mathrm{I}$ (blue solid line), $\phi_{\mathrm{II},0}$ (blue dotted line), and $\phi_{\mathrm{II},1}$ (blue dashed line). Also shown is the optimal angle $\phi = \phi_\mathrm{I} = \phi_\mathrm{II}$ for strategy with fixed input probe states (red dot-dashed line).

## 6.3 Probing with entangled states

We now switch our attention to protocols exploiting entangled two-qubit probe states. The first such scheme is shown in Fig. 6.2(a). Here a measurement is performed on each qubit of a fixed two-qubit probe state $|\Psi\rangle$. The success probability of this protocol can be written as

$$P_\mathrm{succ} = \frac{1}{2} \sum_{x=0}^{1} \sum_{y=0}^{1} \mathrm{Tr}[\Psi \Pi_{f(x,y),x} \otimes \Pi_{f(x,y),y}]. \tag{6.17}$$

This can be rewritten as $P_\mathrm{succ} = \mathrm{Tr}[\Psi R_\mathrm{ent}]$ where

$$R_\mathrm{ent} = \frac{1}{2} \sum_{x=0}^{1} \sum_{y=0}^{1} \Pi_{f(x,y),x} \otimes \Pi_{f(x,y),y}. \tag{6.18}$$

The maximum achievable success probability can be thus determined by calculating the maximum eigenvalue $r_\mathrm{ent,max}$ of $R_\mathrm{ent}$ for all sixteen functions $f(x,y)$ and taking the maximum value. Since $R$ is a $4 \times 4$ matrix, this optimization can be performed fully analytically.

It turns out that two different guessing strategies are optimal depending on the value of $\theta$. For $\theta \leq \theta_\mathrm{th} = \arccos \frac{1}{\sqrt{3}}$ the optimal function $f$ reads

$$f(0,0) = A, \quad f(0,1) = B, \quad f(1,0) = B, \quad f(1,1) = A. \tag{6.19}$$

The optimal (unnormalized) probe state has the form

$$|\Psi\rangle = \cos(2\theta)[|11\rangle - |00\rangle] + (1 - \sin(2\theta))[|01\rangle + |10\rangle], \tag{6.20}$$

and the success probability reads

$$P_{\text{succ,ent}} = \frac{1}{2}[1 + \sin(2\theta)]. \tag{6.21}$$

For $\theta \geq \theta_{\text{th}}$ the symmetry is broken and the optimal $f(x,y)$ is given by

$$f(0,0) = A, \quad f(0,1) = B, \quad f(1,0) = A, \quad f(1,1) = A. \tag{6.22}$$

The corresponding optimal probe state can be expressed as

$$\begin{aligned}|\Psi\rangle &= |00\rangle - |11\rangle + \tan\theta|10\rangle \\ &\quad - \frac{\cos\theta\sqrt{3 + \cos(2\theta)}}{\sqrt{2} + \sin\theta\sqrt{3 + \cos(2\theta)}}|01\rangle,\end{aligned} \tag{6.23}$$

and yields a success probability

$$P_{\text{succ,ent}} = \frac{1}{2}\left(1 + \sqrt{1 - \cos^4\theta}\right), \tag{6.24}$$

which coincides with $P_{\text{succ}}$ achievable by adaptive strategy with single-qubit probes.

The most advanced among the studied strategies employs entanglement and feed-forward, as illustrated in Fig. 6.2(b). A measurement is performed on one part of the entangled two-qubit state and the measurement outcome $x$ determines the unitary operation performed on the second qubit before it is measured.[152] The two measurement results are then used to identify the measurement device as A or B according to a function $f(x,y)$. Without any loss of generality we can assume that for $x = 0$ the operation on the second qubit is an identity transformation while for $x = 1$ a unitary operation $U$ is applied to the qubit. The success rate of the scheme can be expressed as

$$\begin{aligned}P_{\text{succ}} &= \frac{1}{2}\sum_{y=0}^{1}\text{Tr}[\Psi\Pi_{f(0,y),0} \otimes \Pi_{f(0,y),y}] \\ &\quad + \frac{1}{2}\sum_{y=0}^{1}\text{Tr}[\Psi\Pi_{f(1,y),1} \otimes U^{\dagger}\Pi_{f(1,y),y}U].\end{aligned} \tag{6.25}$$

In order to determine the maximum achievable $P_{\text{succ}}$ we have to calculate the maximum eigenvalue $r_{\text{ff,max}}$ of the operator

$$R_{\text{ff}} = \frac{1}{2}\sum_{y=0}^{1}\left(\Pi_{f(0,y),0} \otimes \Pi_{f(0,y),y} + \Pi_{f(1,y),1} \otimes U^{\dagger}\Pi_{f(1,y),y}U\right), \tag{6.26}$$

and further maximize $r_{\text{ff,max}}$ over all single-qubit unitary operations $U$. A thorough numerical optimization reveals that for $\theta < \frac{\pi}{4}$ the feed-forward does not provide any advantage and it is optimal to use the entangled state (6.20) without any feed-forward which leads to the success probability (6.21). The situation, however, changes dramatically for $\theta > \frac{\pi}{4}$. If $\theta \in [\frac{\pi}{4}, \frac{\pi}{2}]$ then the two measurements can be perfectly and deterministically discriminated from two utilizations. The optimal $f(x, y)$ is given by Eq. (6.19). An analytical expression for the required entangled probe state can be derived,

$$|\Psi\rangle = \alpha|00\rangle + \beta|10\rangle + \gamma|11\rangle, \tag{6.27}$$

where

$$
\begin{aligned}
\alpha &= \frac{1}{\sqrt{2}}\sqrt{1 - \sqrt{1 - \frac{1}{\tan^2\theta}}}, \\
\gamma &= -\frac{1}{\sqrt{2}\tan\theta}\sqrt{1 + \sqrt{1 - \frac{1}{\tan^2\theta}}}, \\
\beta &= -\frac{\alpha}{\tan\theta} - \gamma\tan\theta.
\end{aligned} \tag{6.28}
$$

The conditional unitary operation $U$ on the second qubit that should be applied if the outcome of the first measurement reads 1 is defined as follows,

$$
\begin{aligned}
U|0\rangle &= \frac{1}{\sqrt{\beta^2 + \gamma^2}}(\gamma|0\rangle + \beta|1\rangle), \\
U|1\rangle &= \frac{1}{\sqrt{\beta^2 + \gamma^2}}(-\beta|0\rangle + \gamma|1\rangle).
\end{aligned} \tag{6.29}
$$

The obtained results are illustrated in Fig. 6.4 that shows the dependence of $P_{\text{succ}}$ on $\theta$ for the four studied discrimination strategies. We can see that adaptive strategy, entanglement and feed-forward all help to increase the success probability of the discrimination. For $\theta < \theta_{\text{th}}$ the strategy based on a fixed entangled probe outperforms the adaptive strategy with single-qubit probe states. Interestingly, in the interval $\theta \in [\frac{\pi}{4}, \theta_{\text{th}}]$ the success probability of strategy involving fixed entangled probe decreases with increasing $\theta$, c.f. dashed green line in Fig. 6.4. This somewhat surprising feature arises because the class of discrimination strategies with fixed entangled probes represents only a subset of all possible strategies. By restricting ourselves to this class of strategies we impose certain constraints which in this particular case give rise to the non-monotonicity of $P_{\text{succ,ent}}$. If we employ a more
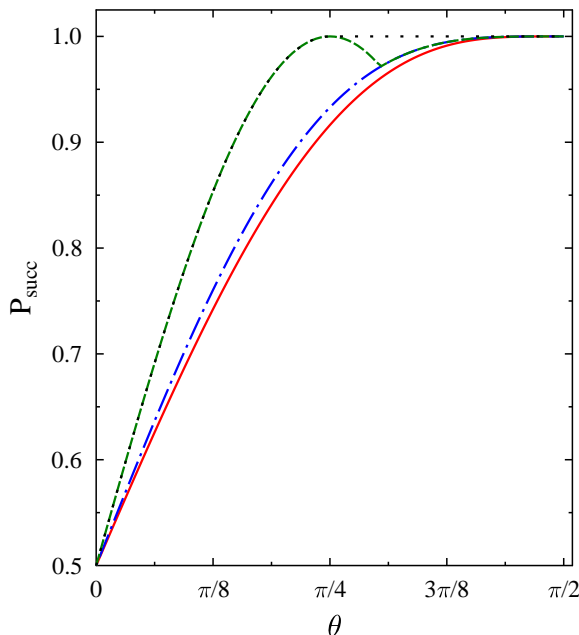
Figure 6.4: Dependence of the success probability of the measurement discrimination $P_{\text{succ}}$ on the angle $\theta$ is plotted for four different discrimination strategies: probing with fixed separable states (solid red line), adaptive strategy employing separable states (dot-dashed blue line), probing with entangled state (dashed green line), and combination of entangled probe state and a feed-forward (dotted black line).

general discrimination strategy combining entangled probe and feed-forward then we recover the intuitively expected monotonic dependence of $P_{\text{succ}}$ on $\theta$. Moreover, with this latter method the two quantum measurements can be perfectly deterministically discriminated[152] when $\theta \geq \frac{\pi}{4}$.

## 6.4   Experiment

In order to test the above developed discrimination strategies, we have experimentally implemented discrimination of projective measurements on a polarization state of a single photon. In the experiment, the alternative A corresponds to the measurement in the basis of horizontally/vertically polarized single-photon states, $(|H\rangle, |V\rangle)$, while the alternative B represents a measurement in the basis of linearly polarized states rotated by angle $\theta$ with respect to the $H/V$ basis, $(\cos\theta|H\rangle + \sin\theta|V\rangle,$
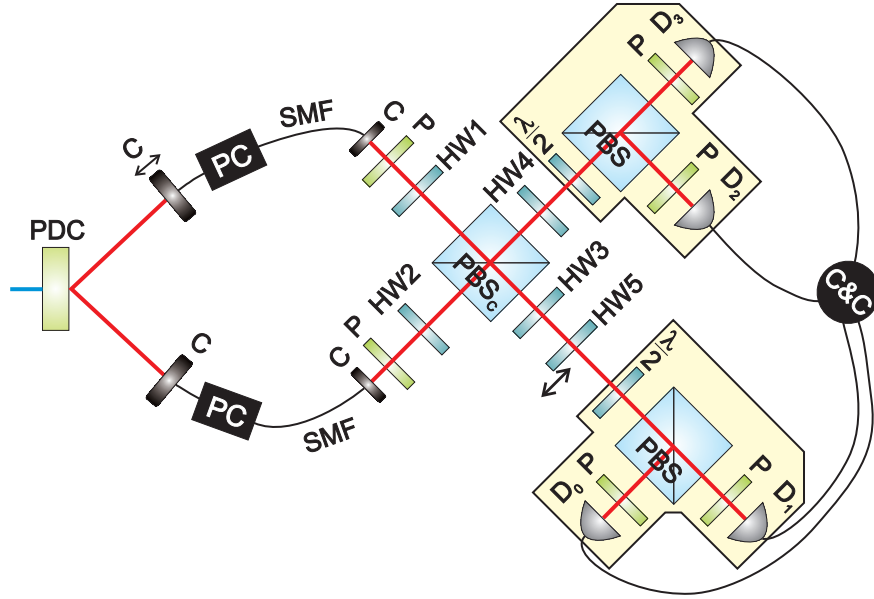
Figure 6.5: Experimental setup. The scheme consists of a nonlinear crystal where pairs of photons are generated in the process of spontaneous parametric down conversion (PDC), single-mode fibers (SMF), fiber polarization controllers (PC), fiber in/out couplers (C), bulk polarizers (P), half-wave plates (HW, $\lambda/2$), polarizing beam splitters (PBS), single-photon detectors (D), and coincidence electronics (C&C). The half-wave plate HW5 was inserted in the setup only for measurements with entangled probe states.

$\sin\theta|H\rangle - \cos\theta|V\rangle$). As shown in Fig. 6.5, the measurement block consists of a half-wave plate ($\frac{\lambda}{2}$) whose rotation angle defines the measurement basis, polarizing beam splitter (PBS), two polarizers (P) and two avalanche photodiodes serving as single-photon detectors (D). The polarizers in front of the detectors filter out any possible remaining undesired signal that could be present due to imperfections of the PBS. Similarly as in Ref.,[165] we make use of spatial multiplexing, where two physical copies of the measuring apparatus are available. Note that this is merely a technical simplification of the experiment and all the developed discrimination strategies can be implemented also with only a single apparatus by using time multiplexing and delay lines.

In our experiment, pairs of temporally correlated horizontally polarized photons are generated in the process of frequency degenerate Type-I non-collinear parametric downconversion in a LiIO$_3$ crystal pumped by a cw laser diode emitting 40 mW of power at the wavelength of 407 nm.[?] The downconverted signal and idler photons

at wavelength 814 nm are spatially filtered by coupling them into single mode fibers. After release into free space, the polarization states of the photons can be set and controlled by polarizers P and half-wave plates HW1 and HW2. The photons then impinge onto a polarizing beam splitter $\text{PBS}_C$ and propagate through additional half-wave plates HW3, HW4 (and, optionally, HW5) before impinging onto the two detection blocks. The central polarizing beam splitter $\text{PBS}_C$ together with the wave plates provide sufficient flexibility necessary for the implementation of the various discrimination strategies including those which require preparation of specific entangled states.

We begin by implementation of the strategy employing two equally polarized single-photon probes. The wave plates HW1 and HW2 are set to 0° such that both signal and idler photons are horizontally polarized and are fully transmitted through $\text{PBS}_C$. The half-wave plates HW3 and HW4 are rotated such as to prepare both photons in pure linear polarization state $|\psi\rangle = \cos\phi_\text{I}|H\rangle + \sin\phi_\text{I}|V\rangle$, where the angle $\phi_\text{I}$ is given by Eq. (6.10). The photons are then detected by the measurement blocks and the coincidences between clicks of one detector from each block are recorded. Following Eq. (6.8), if the coincidences D0&D2, D0&D3, or D1&D2 are observed then we guess that the apparatus performs measurement in the H/V basis (device A), while if the coincidence D1&D3 is recorded then we conclude that the apparatus performs measurement in the rotated basis (device B). We measure the coincidences for both basis settings and from the experimental data we calculate the success probability of a correct guess assuming that the *a-priori* probability of each measurement device A or B was $\frac{1}{2}$.

We then proceed to the adaptive discrimination strategy. In the present proof-of-principle experiment, we were not able to realize real-time adaptive measurement strategy, but we nevertheless successfully emulated this approach as follows. For both devices A and B (i.e. both basis settings) we perform two measurements. First, the signal photon is prepared by HW3 in a linearly polarized state at angle $\phi_\text{I} = \frac{\pi}{4} + \frac{\theta}{2}$, cf. Eq. (6.15), the idler photon is prepared by HW4 in a linearly polarized state $\cos\phi_{\text{II},0}|H\rangle + \sin\phi_{\text{II},0}|V\rangle$, and the four coincidences are measured. The second measurement is almost identical to the first one except that the idler photon is prepared in a state $\cos\phi_{\text{II},1}|H\rangle + \sin\phi_{\text{II},1}|V\rangle$. From the first (second) measurement we take into account only coincidences D0&D2 and D0&D3 (D1&D2 and D1&D3). The success probabilities are then calculated from this combined experimental data and according to the identification pattern (6.14).

The entanglement-based strategies are much more experimentally demanding

because the two photons have to be prepared in an entangled state whose quality depends on the visibility of two-photon interference on $\text{PBS}_C$. First we address the simpler strategy without feed-forward. The probe state (6.20) is actually maximally entangled and can be rewritten as,

$$
\begin{aligned}
|\Psi\rangle \;=\;& |H\rangle[(\cos\theta - \sin\theta)|V\rangle - (\cos\theta + \sin\theta)|H\rangle] \\
&+|V\rangle[(\cos\theta + \sin\theta)|V\rangle + (\cos\theta - \sin\theta)|H\rangle].
\end{aligned}
\tag{6.30}
$$

We rotate HW1 and HW2 by 22.5° to prepare both signal and idler photons in front of $\text{PBS}_C$ in diagonally polarized state $\frac{1}{\sqrt{2}}(|H\rangle + |V\rangle)$. The two-photon state right at the output of $\text{PBS}_C$ conditional on a single photon propagating in each arm is maximally entangled and reads $\frac{1}{\sqrt{2}}(|HH\rangle + |VV\rangle)$. This state can be transformed into the desired state (6.30) by rotating the wave plates HW3 and HW4. In order to compensate for an unwanted $\pi$ phase shift we also insert an additional half-wave plate HW5 into the setup. We measure coincidences for both measurement bases and determine the probability of successful discrimination from the acquired data.

Finally, we test the strategy involving entangled states and feed-forward. Since a fast feed-forward loop was not at our disposal we have decided to emulate this strategy similarly as in the case of adaptive strategy. We have determined setting of the wave plates HW1–HW5 which yields the partially entangled two-photon probe state (6.27). For a given fixed $\theta$ we measure coincidences for both measurement bases and then we rotate half-wave plate HW4 such that this operation is equivalent to the feed-forward transformation $U$, cf. Eq. (6.29). We repeat all measurements for this altered configuration. From the first set of data we extract coincidences D0&D2 and D0&D3 and from the second set of data we use coincidences D1&D2 and D1&D3. This yields the same data as a true feed-forward scheme where the rotation of the wave plate HW4 is performed only when detector D1 clicks and before the idler photon passes through HW4.

The experimentally determined success probabilities for all four strategies are shown in Fig. 6.6. The results agree very well with the theoretical predictions. The statistical error of the measured $P_{\text{succ}}$ is below $2 \times 10^{-3}$. The error bars are smaller than the sizes of the symbols used in the graph and are thus not plotted. As predicted, the adaptive scheme outperforms the scheme with fixed single-qubit probe states, and the use of entangled states further significantly improves the probability of successful discrimination. We can see that for $\theta > \theta_{\text{th}} \approx 54.7°$ the entangled state
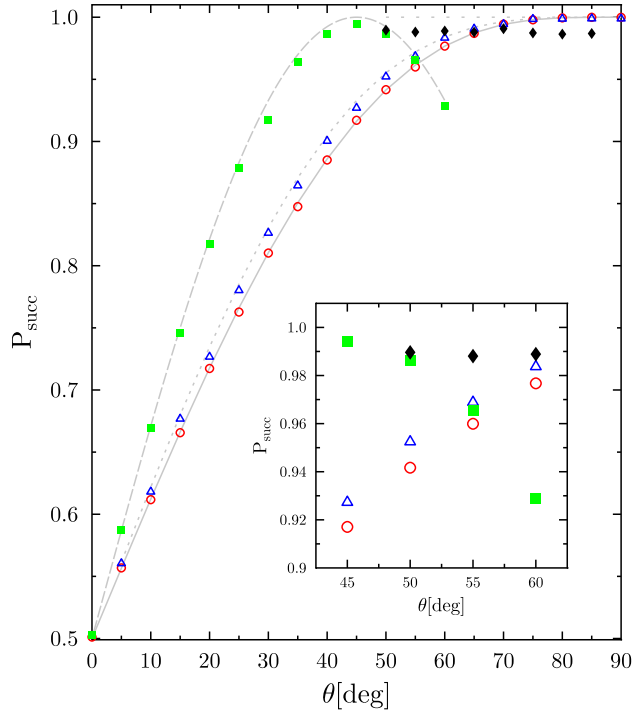
Figure 6.6: Experimental results. Experimentally determined probability of successful discrimination $P_{\text{succ}}$ is plotted for four different discrimination strategies: strategy with fixed single-qubit probes ($\circ$), adaptive strategy with single qubit probes ($\triangle$), strategy employing two-qubit entangled state (6.30) ($\blacksquare$, measurements made for $0° \leq \theta \leq 60°$) and strategy combining entanglement and feed-forward ($\blacklozenge$, measurements made for $50° \leq \theta \leq 85°$). The thin grey lines show the corresponding theoretical curves. The inset shows details around $\theta = 55°$.

(6.20) ceases to be optimal as expected. The discrepancy between theory and experiment is larger for entanglement-based strategies than for strategies with separable probes, because the performance of the former is affected by less-than unit visibility of two-photon interference on $\text{PBS}_C$ (we measure $V = 0.98$) and the imperfections of $\text{PBS}_C$. Nevertheless, the strategy combining entanglement and feed-forward consistently achieves success probability $\approx 99\%$ for $\theta \in (50°, 85°)$. In particular, for $\theta = 55°$ the advantage of using the entanglement and feed-forward is clearly visible from the experimental results, cf. inset in Fig. 6.6. As $\theta$ approaches $90°$ the strategies involving separable probe states eventually outperform the entanglement-based strategy because they are much less affected by the technical imperfections.

## 6.5  Conclusions

In this chapter we have studied the discrimination between two projective single-qubit quantum measurements. We have seen that if two applications of the measurement are possible, then there exist several different discrimination strategies of varying complexity and performance. We have found that adaptive strategy, entanglement and feed-forward all help to increase the success probability of the discrimination. We have explicitly determined an entangled probe state that, together with feed-forward, enables perfect deterministic two-copy discrimination of the two measurements for $\frac{\pi}{4} \leq \theta \leq \frac{\pi}{2}$. This is analogous to the perfect finite-copy distinguishability of unitary transformations and general quantum operations.[148, 152, 157] We have successfully experimentally confirmed the performance of the investigated protocols using a linear optical scheme where the task was to discriminate between two different measurements on a polarization state of single photon.

The discrimination scenarios considered in this chapter did not involve any other ancilla measurements in addition to the measurement $M$ that should be discriminated. If we allow for such additional ancilla measurements then we can in principle construct even more sophisticated discrimination schemes that can be described by the formalism of quantum combs.[166, 167] Investigation of such advanced strategies as well as strategies involving inconclusive outcomes[153] is left for future work.

# Chapter 7

# Conclusions and outlook

One of the goals of quantum optics is to design and implement new sources of quantum light, which could enable tunable control of the relevant photonic properties as required by the specific quantum information applications under consideration. To date most quantum information applications use the polarization of photons, or polarization entanglement between paired photons, as the quantum resource. In this thesis we have presented research in the field of preparation of different correlated photon pairs via SPDC and their use in quantum information processing experiments.

In chapter 4, we have proposed and experimentally verified source of entangled photon pairs with tunable frequency correlations. We have used pulse front tilt technique to control the type of frequency correlations and the bandwidth of entangled photon pairs generated by spontaneous parametric downconversion in a nonlinear crystal pumped by femtosecond laser pulses. The technique allows us to produce frequency correlations, anticorrelations or nocorrelations at will. The essence of the pulse front tilt technique is to modify effective group velocities and effective group velocity dispersions of all the interacting fields (for example by a diffraction grating) inside the nonlinear medium. We have applied direct and indirect measurement of frequency correlations to characterize different regimes of frequency generation from single nonlinear crystal. An additional advantage of the pulse front tilt technique is that it can be used in any nonlinear material and at frequency bandwidths where standard solutions cannot be applied.

Chapter 5 is dedicated to experimental realization of a programmable quantum phase gate. This simple quantum processor applies a unitary phase shift operation to the data qubit with the value of the phase shift being fully determined by the

state of the program qubit. The experimental setup employed linear optical implementation based on encoding of qubits into polarization states of single photons, two-photon interference on a polarizing beam splitter, and measurement on the output program qubit. We have characterized the programmable quantum gate by full quantum process tomography. We have also demonstrated that with a different set of program states, the device can also operate as a programmable partial polarization filter. This simple quantum gate can serve as a basic building block of more complex multiqubit linear-optics quantum gates or other optical quantum information processing devices.

Finally, in chapter 6, we have proposed optimal two-copy discrimination between two projective quantum measurements on a single qubit. We have considered discrimination scenarios where the measurement that should be identified can be performed only twice and did not involve any other ancilla measurements in addition to the measurement that should be discriminated. We have showed that adaptive discrimination strategy, entangled probe states, and feed-forward all help to increase the probability of correct identification of the measurement. With use of linear optics we have successfully experimentally demonstrated all the presented discrimination strategies. The employed experimental setup involves projective measurements on polarization states of single photons and preparation of required probe two-photon polarization states by the process of spontaneous parametric down-conversion and passive linear optics.

In regard to our ongoing and planned activities, we are currently working on the Toffoli gate, which is a three qubit entangling gate that flips the logical state of the target qubit conditionally on the logical state of the two control qubits. Our optical implementation is based on the encoding of qubits into polarization and spatial degrees of freedom of single photons. We are using inherently phase stable Mach-Zehnder interferometer for encoding the spatial degree of freedom. Another ongoing project focuses on losses suppression in optical quantum communication using combination of noiseless amplification and reversible losses. The optical implementation is based on realized programmable quantum phase gate and beam splitter with variable beam splitting ratio for both polarization modes.

# Stručné shrnutí v češtině

Cílem disertační práce je prezentace vědeckých výsledků na poli generace korelovaných párů fotonů získaných pomocí spontánní parametrické frekvenční sestupné konverze a jejich využití v experimentálním kvantovém zpracování informace.

V první části disertační práce se věnujeme přípravě různých typů frekvenčních korelací kvantově provázaných fotonových párů generovaných pomocí spontánní parametrické frekvenční sestupné konverze. Experimentálně zde demonstrujeme úplnou kontrolu frekvenčních korelací kvantově provázaných párů fotonů pomocí metody naklonění čela pulzu. Metoda je založena na správném nastavení grupových rychlostí všech interagujících vln v nelineárním prostředí. K tomuto účelu se využívají svazky ovlivněné prostředím s úhlovou disperzí, jako je například difrakční mřížka. Nelineární prostředí je čerpané pomocí femtosekundových pulzů přičemž není potřeba použít žádné úzkopásmové frekvenční filtry. Byla implementována dvě experimentální uspořádání, jedno pro přímé a druhé pro nepřímé měření frekvenčních korelací, přičemž oba experimenty jasně prokazují flexibilitu a univerzalitu této techniky. Nejprve demonstrujeme generaci frekvenčních antikorelací kvantově provázaných párů fotonů. Dále ukazujeme, jak lze generovat frekvenčně korelované kvantově provázané páry fotonů, které mohou najít uplatnění například v kvantové metrologii. Posledním speciálním případem je generace frekvenčně zcela nekorelovaných párů fotonů. Je potřeba zdůraznit, že experimentálně demonstrované typy frekvenčních korelací jsou jen speciální případy všech korelací a šířek spektra, které lze s touto metodou dosáhnout. Metoda, kterou používáme, je nezávislá na vlnové délce a nelineárním prostředí, proto může být využita i tam, kde jiné řešení není k dispozici.

V další části práce se zabýváme experimentální demonstrací programovatelného jednoqubitového kvantového fázového hradla. Tento kvantový procesor aplikuje unitární operaci fázového posuvu na datový qubit, přičemž tato operace je plně zakódována do stavu programového qubitu. Experimentální realizace jednoqubitového fázového hradla je založena na kódování qubitů do polarizačních stavů jednotlivých

fotonů, dvoufotonové interferenci na polarizačním děliči svazku a následném měření výstupního programového qubitu. Programovatelné jednoqubitové fázové hradlo jsme charakterizovali pomocí úplné tomografie kvantového procesu. Dále jsme ukázali, že změnou programových stavů lze zařízení využít jako programovatelný částečný polarizační filtr.

V závěrečné části práce se věnujeme optimální diskriminaci mezi dvěma projekčními kvantovými měřeními na jednom qubitu. Uvažujeme případ, kdy měření, které má být identifikováno, může být provedeno pouze dvakrát. Studované diskriminační strategie experimentálně demonstrujeme a testujeme jejich úspěšnost. Experiment využívá spontánní parametrickou sestupnou frekvenční konverzi pro přípravu požadovaných testovacích dvoufotonových polarizačních stavů, pasivní lineární optiku a projekční měření do polarizačních stavů jednotlivých fotonů. Ukazujeme zde, že adaptivní diskriminační strategie, kvantově provázané testovací stavy a zpětná vazba mohou zvýšit pravděpodobnost správné identifikace projekčního měření.

# Publications and citations

■ M. Hendrych, M. Mičuda, J. P. Torres, *Tunable control of the frequency correlations of entangled photons*, Opt. Lett. **32**, 2339 (2007).

■ M. Mičuda, O. Haderka, M. Ježek, *High-efficiency photon-number-resolving multichannel detector*, PRA **78**, 025804 (2008).

■ M. Mičuda, M. Ježek, M. Dušek, J. Fiurášek, *Experimental realization of a programmable quantum gate*, Phys. Rev. A **78**, 062311 (2008).

■ J. Fiurášek, M. Mičuda, *Optimal two-copy discrimination of quantum measurements*, Phys. Rev. A **80**, 042312 (2009).

■ M. Hendrych, M. Mičuda, J. P. Torres, *Tunable control of the frequency correlations of entangled photons*, Opt. Lett. **32**, 2339 (2007).

1. S.Y. Baek, O. Kwon, and Y. H. Kim, *Temporal shaping of a heralded single-photon wave packet*, Phys. Rev. A **77**, 013829 (2008).

2. X. Shi, A. Valencia, M. Hendrych, and J. P. Torres, *Generation of indistinguishable and pure heralded single photons with tunable bandwidth*, Opt. Lett. **33**, 875 (2008).

3. O. Kuzucu, F. N. C. Wong, S. Kurimura, and S. Tovstonog, *Joint Temporal Density Measurements for Two-Photon State Characterization*, Phys. Rev. Lett. **101**, 153602 (2008).

4. M. Hendrych, X. Shi, A. Valencia, and J. P. Torres, *Broadening the bandwidth of entangled photons: A step towards the generation of extremely short biphotons*, Phys. Rev. A **79**, 023817 (2009).

5. Y. Jeronimo-Moreno and A. B. URen, *Control, measurement, and propagation of entanglement in photon pairs generated through type-II parametric down-conversion*, Phys. Rev. A **79**, 033839 (2009).

6. V. Torres-Company, A. Valencia, and J. P. Torres, *Tailoring the spectral coherence of heralded single photons*, Opt. Lett. **34**, 1177 (2009).

7. P. Abolghasem, M. Hendrych, X. Shi, J. P. Torres, and A. S. Helmy, *Bandwidth control of paired photons generated in monolithic Bragg reflection waveguides*, Opt. Lett. **34**, 2000 (2009).

8. R. Shimizu and K. Edamatsu, *High-flux and broadband biphoton sources with controlled frequency entanglement*, Opt. Express **17**, 16385 (2009).

9. P. Abolghasem, X. Shi, M. Hendrych, J. P. Torres, and A. S. Helmy, *Bragg Reflection Waveguides: A Novel Platform for Enhanced Control of Photon-Pair Generation via Spontaneous Parametric Down Conversion*, 2009 CONFERENCE ON LASERS AND ELECTRO-OPTICS AND QUANTUM ELECTRONICS AND LASER SCIENCE CONFERENCE (CLEO/QELS 2009), VOLS **1 − 5**, 2146 (2009).

10. E. V. Luis, A. B. U'Ren, R. Rangarajan, C. I. Osorio, J. P . Torres, L. J. Zhang, I. A. Walmsley, *Design of bright, fiber-coupled and fully factorable photon pair sources*, NEW JOURNAL OF PHYSICS **12**, 093027 (2010).

11. H. Oka, *Efficient two-step up-conversion by quantum-correlated photon pairs*, Opt. Exp. 18, 25839 (2010).

12. K. G. Katamadze, S. P. Kulik, *Control of the spectrum of the biphoton field*, JOURNAL OF EXPERIMENTAL AND THEORETICAL PHYSICS 112, 20 (2011).

13. J. Svozilik, M. Hendrych, A. S. Helmy, J. P. Torres, *Generation of paired photons in a quantum separable state in Bragg reflection waveguides*, Opt. Exp. 19, 3115 (2011).

14. A. S. Helmy, P. Abolghasem, J. S. Aitchison, B. J. Bijlani, J. Han, B. M. Holmes, D. C. Hutchings, U. Younis, S. J. Wagner, *Recent advances in phase matching of second-order nonlinearities in monolithic semiconductor waveguides*, LASER & PHOTONICS REVIEWS 5, 272 (2011).

15. H. Oka, *Selective two-photon excitation of a vibronic state by correlated photons*, JOURNAL OF CHEMICAL PHYSICS 134, 124313 (2011).

■   M. Mičuda, O. Haderka, M. Ježek, *High-efficiency photon-number-resolving multichannel detector*, Phys. Rev. A **78**, 025804 (2008).

1. A. Andreoni and M. Bondani, *Photon statistics in the macroscopic realm measured without photon counters*, Phys. Rev. A **80**, 013819 (2009).

2. J. Fiurášek, *Engineering quantum operations on traveling light beams by multiple photon addition and subtraction*, Phys. Rev. A **80**, 053822 (2009).

3. A. Andreoni, A. Allevi, and M. Bondani, *Photon-number statistics measured with a noncounting PMT*, JOURNAL OF RUSSIAN LASER RESEARCH **30**, 418 (2009).

4. M. Bondani, A. Allevi, A. Andreoni, *Light Statistics by Non-Calibrated Linear Photodetectors*, ADVANCED SCIENCE LETTERS **2**, 463 (2009).

5. P. Huang, Y. Lu, G. Zeng, *A novel nondeterministic scheme for a nondestructive two-qubit controlled phase gate with linear optics*, Phys. Lett. A **374**, 527 (2010).

6. M. Ramilli, A. Allevi, V. Chmill, M. Bondani, M. Caccia, A. Andreoni, *Photon-number statistics with silicon photomultipliers*, JOURNAL OF THE OPTICAL SOCIETY OF AMERICA B-OPTICAL PHYSICS 27, 852 (2010).

7. A. Allevi, M. Bondani, A. Andreoni, *Photon-number correlations by photon-number resolving detectors*, Opt. Lett. 35, 1707 (2010).

8. M. Bondani, A. Allevi, A. Andreoni, *CHOOSING A PHOTOEMISSIVE DETECTOR SUITABLE FOR PHOTON-NUMBER STATISTICS OF PULSED FIELDS*, INTERNATIONAL JOURNAL OF QUANTUM INFORMATION 9, 93 (2011).

9. A. Allevi, F. A. Beduini, M. Bondani, A. Andreoni, *PHOTON-NUMBER CORRELATION OF A CLASSICAL EXOTIC STATE IN THE MESOSCOPIC REGIME*, INTERNATIONAL JOURNAL OF QUANTUM INFORMATION 9, 103 (2011).

10. D. A. Kalashnikov, S. H. Tan, M. V. Chekhova, L. A. Krivitsky, *Accessing photon bunching with a photon number resolving multi-pixel detector*, Opt. Exp. 19, 9352 (2011).

■   M. Mičuda, M. Ježek, M. Dušek, J. Fiurášek, *Experimental realization of a programmable quantum gate*, Phys. Rev. A **78**, 062311 (2008).

1. L. Slodička, M. Ježek, J. Fiurášek, *Experimental demonstration of a teleportation-based programmable quantum gate*, Phys. Rev. A **79**, 050304 (2009).

2. M. Hillery, V. Bužek, *Quantum machines*, CONTEMPORARY PHYSICS **50**, 575 (2009).

3. M. Hillery, V. Bužek, M. Ziman, *Equivalent programmable quantum processors*, OPTICS COMMUNICATIONS **283**, 822 (2010).

4. S. Levente, K. Matyas, A. Peter, J. Jozsef, *Optimal universal asymmetric covariant quantum cloning circuits for qubit entanglement manipulation*, Phys. Rev. A 81, 032323 (2010).

5. X.-C. Yao, J. Fiurasek, H. Lu, W.-B. Gao, Y.-A. Chen, Z.-B. Chen,J.-W. Pan, *Experimental Realization of Programmable Quantum Gate Array for Directly Probing Commutation Relations of Pauli Operators*, Phys. Rev. Lett. 105, 120402 (2010).

■ J. Fiurášek, M. Mičuda, *Optimal two-copy discrimination of quantum measurements*, Phys. Rev. A **80**, 042312 (2009).

# Bibliography

[1] P. D. Maker, R. W. Terhune, and C. M. Savage, *Intensity-Dependent Changes in the Refractive Index of Liquids*, Phys. Rev. Lett. **12**, 507 (1964).

[2] Y. Silberberg, *Photonic switching devices*, Optics News **15**, 7 (1989).

[3] P. A. Franken, A. E. Hill, C. W. Peters, and G. Weinreich, *Generation of Optical Harmonics*, Phys. Rev. Lett. **7**, 118 (1961).

[4] J. S. Bell, *On the Einstein-Podolsky-Rosen Paradox.*, Physics **1**, 195 (1964).

[5] P. G. Kwiat, K. Mattle, H. Weinfurter, and A. Zeilinger, *New High-Intensity Source of Polarization-Entangled Photon Pairs*, Phys. Rev. Lett. **75**, 4337 (1995).

[6] C. K. Law, I. A. Walmsley, and J. H. Eberly, *Continuous Frequency Entanglement: Effective Finite Hilbert Space and Entropy Control*, Phys. Rev. Lett. **84**, 5304 (2000).

[7] A. Mair, A. Vaziri, G. Weihs, and A. Zeilinger, *Entanglement of the orbital angular momentum states of photons*, Nature **412**, 313 (2001).

[8] A. Vaziri, G. Weihs, and A. Zeilinger, *Experimental Two-Photon, Three-Dimensional Entanglement for Quantum Communication*, Phys. Rev. Lett. **89**, 240401 (2002).

[9] C. K. Hong, Z. Y. Ou, and L. Mandel, *Measurement of subpicosecond time intervals between two photons by interference*, Phys. Rev. Lett. **59**, 2044 (1987).

[10] R. Loudon, *The quantum theory of Light*, Oxford Univ. Press (2000).

[11] A. Pe'er, B. Dayan, A. A. Friesem, and Y. Silberberg, *Temporal Shaping of Entangled Photons*, Phys. Rev. Lett. **94**, 073601 (2005).

[12] V. Giovannetti, S. Lloyd, and L. Maccone, *Quantum-enhanced positioning and clock synchronization*, Nature *412*, 417 (2001).

[13] P. P. Rohde, T. C. Ralph, and M. A. Nielsen, *Optimal photons for quantum-information processing*, Phys. Rev. A **72**, 052332 (2005).

[14] W. P. Grice, A. B. U'Ren, and I. A. Walmsley, *Eliminating frequency and space-time correlations in multiphoton states*, Phys. Rev. A **64**, 063815 (2001).

[15] O. Kocuzu, M. Fiorentino, M. A. Albota, F. N. C. Wong, and F. X. Kärtner , *Two-Photon Coincident-Frequency Entanglement via Extended Phase Matching*, Phys. Rev. Lett. **94**, 083601 (2005).

[16] S. Carrasco, J. P. Torres, L. Torner, A. Sergienko, B. E. A. Saleh, and Malvin C. Teich, *Enhancing the axial resolution of quantum optical coherence tomography by chirped quasi-phase matching*, Opt. Lett. **29**, 2429 (2004).

[17] Z. Y. Ou and Y. J. Lu, *Cavity Enhanced Spontaneous Parametric Down-Conversion for the Prolongation of Correlation Time between Conjugate Photons*, Phys. Rev. Lett. **83**, 2556 (1999).

[18] A. B. URen, R. K. Erdmann, M. Cruz-Gutierrez, and I. A. Walmsley, *Generation of Two-Photon States with an Arbitrary Degree of Entanglement Via Nonlinear Crystal Superlattices*, Phys. Rev. Lett. **97**, 223602 (2006).

[19] S. Carrasco, J. P. Torres, and L. Torner, *Spatial-to-spectral mapping in spontaneous parametric down-conversion*, Phys. Rev. A **70**, 043817 (2004); Phys. Rev. A **73**, 063802 (2006).

[20] M. C. Booth, M. Atatre, G. Di Giuseppe, B. E. A. Saleh, A. V. Sergienko, and M. C. Teich, *Counterpropagating entangled photons from a waveguide with periodic nonlinearity*, Phys. Rev. A **66**, 023815 (2002).

[21] A. De Rossi and V. Berger, *Counterpropagating Twin Photons by Parametric Fluorescence*, Phys. Rev. Lett. **88**, 043901 (2002).

[22] Z. D. Walton, M. C. Booth, A. V. Sergienko, B. E. A. Saleh, and M. C. Teich, *Controllable frequency entanglement via auto-phase-matched spontaneous parametric down-conversion*, Phys. Rev. A **67**, 053810 (2003).

[23] A. B. U'Ren, K. Banaszek, I. A. Walmsley, *Photon engineering for quantum information processing* , Quantum Inf. Comput. **3**, 480 (2003).

[24] X.-C. Yao, T.-X. Wang, P. Xu, H. Lu, G.-S. Pan, X.-H. Bao, C.-Z. Peng, C.-Y. Lu, Y.-A. Chen, J.-W. Pan, *Observation of eight-photon entanglement*, arXiv: 1105.6318v1 [quant-ph] (2011).

[25] D. P. DiVincenzo, *Quantum Computation*, Science **13**, 255 (1995).

[26] C. H. Bennett, *Quantum Information and Computation*, Phys. Today **48**, No. 10, 24 (1995).

[27] A. Ekert and R. Jozsa, *Quantum computation and Shors factoring algorithm*, Rev. Mod. Phys. **68**, No. 3, 733 (1996).

[28] L. K. Grover, *Quantum Mechanics Helps in Searching for a Needle in a Haystack*, Phys. Rev. Lett. **79**, 325 (1997).

[29] P. W. Shor, *Polynomial-time algorithms for prime factorization and discrete logarithms on a quantum computer*, SIAM J. Computing **26**, 1484 (1997).

[30] M.A. Nielsen and I.L. Chuang, *Quantum Computation and Quantum Information* (Cambridge University Press, Cambridge, 2000).

[31] T. Toffoli, *Reversible Computing*, Tech. Memo MIT/LCS/TM-151, MIT Lab. for Com. Sci. (1980).

[32] Y. Shi, *Both Toffoly and controled-NOT need little help to do universal quantum computation*, Quantum Inform. Comput. **3**, 84 (2003).

[33] D. G. Cory, M. D. Price, W. Maas, E. Knill, R. Laflamme, W. H. Zurek, T. F. Havel, and S. S. Somaroo, *Experimental Quantum Error Correction*, Phys. Rev. Lett. **81**, 2152 (1998).

[34] E. Dennis, *Toward fault-tolerant quantum computation without concatenation*, Phys. Rev. A **63**, 052314 (2001).

[35] T. Sleator and H. Weinfurter, *Realizable Universal Quantum Logic Gates*, Phys. Rev. Lett. **74**, 4087 (1995).

[36] A. Barenco, *A universal two-bit gate for quantum computation*, Proc. R. Soc. Lond. A **449**, 679 (1995).

[37] G. J. Milburn, *Quantum optical Fredkin gate*, Phys. Rev. Lett. **62**, 2124 (1989).

[38] E. Knill, R. Laflamme, and G. J. Milburn, *A scheme for efficient quantum computation with linear optics*, Nature **409**, 46 (2001).

[39] M. Koashi, T. Yamamoto, and N. Imoto, *Probabilistic manipulation of entangled photons*, Phys. Rev. A **63**, 030301(R) (2001).

[40] T. B. Pittman, B. C. Jacobs, and J. D. Franson, *Probabilistic quantum logic operations using polarizing beam splitters*, Phys. Rev. A **64**, 062311 (2001).

[41] T. C. Ralph, A. G. White, W. J. Munro, and G. J. Milburn, *Simple scheme for efficient linear optics quantum gates*, Phys. Rev. A **65**, 012314 (2001).

[42] T. C. Ralph, N. K. Langford, T. B. Bell, and A. G. White, *Linear optical controlled-NOT gate in the coincidence basis*, Phys. Rev. A **65**, 062324 (2002).

[43] H. F. Hofmann and S. Takeuchi, *Quantum phase gate for photonic qubits using only beam splitters and postselection*, Phys. Rev. A **66**, 024308 (2002).

[44] E. Knill, *Quantum gates using linear optics and postselection*, Phys. Rev. A **66**, 052306 (2002).

[45] J. Fiurášek, *Linear-optics quantum Toffoli and Fredkin gates*, Phys. Rev. A **73**, 062313 (2006).

[46] J. Fiurášek, *Linear optical Fredkin gate based on partial-SWAP gate*, Phys. Rev. A **78**, 032317 (2008).

[47] P. Marek and J. Fiurášek, *Elementary gates for quantum information with superposed coherent states*, Phys. Rev. A **82**, 014304 (2010).

[48] K. Sanaka, K. Kawahara, and T. Kuga, *Experimental probabilistic manipulation of down-converted photon pairs using unbalanced interferometers*, Phys. Rev. A **66**, 040301(R) (2002).

[49] T. B. Pittman, B. C. Jacobs, and J. D. Franson, *Demonstration of Nondeterministic Quantum Logic Operations Using Linear Optical Elements*, Phys. Rev. Lett. **88**, 257902 (2002).

[50] T. B. Pittman, M. J. Fitch, B. C Jacobs, and J. D. Franson, *Experimental controlled-NOT logic gate for single photons in the coincidence basis*, Phys. Rev. A **68**, 032316 (2003).

[51] J. L. O'Brien, G. J. Pryde, A. G. White, T. C. Ralph, and D. Branning, *Demonstration of an all-optical quantum controlled-NOT gate*, Nature **426**, 264 (2003).

[52] K. Sanaka, T. Jennewein, J.-W. Pan, K. Resch, and A. Zeilinger, *Experimental Nonlinear Sign Shift for Linear Optics Quantum Computation*, Phys. Rev. Lett. **92**, 017902 (2004).

[53] S. Gasparoni, J.-W. Pan, P. Walther, T. Rudolph, and A. Zeilinger, *Realization of a Photonic Controlled-NOT Gate Sufficient for Quantum Computation*, Phys. Rev. Lett. **93**, 020504 (2004).

[54] M. Fiorentino and F. N. C. Wong, *Deterministic Controlled-NOT Gate For Single-Photon Two-Qubit Quantum Logic*, Phys. Rev. Lett. **93**, 070502 (2004).

[55] J. L. O'Brien, G. J. Pryde, A. Gilchrist, D. F. V. James, N. K. Langford, T. C. Ralph, and A. G. White, *Quantum Process Tomography of a Controlled-NOT Gate*, Phys. Rev. Lett. 93, 080502 (2004).

[56] Z. Zhao, A.-N. Zhang, Y.-A. Chen, H. Zhang, J.-F. Du, T. Yang, and J.-W. Pan, *Experimental Demonstration of a Nondestructive Controlled-NOT Quantum Gate for Two Independent Photon Qubits*, Phys. Rev. Lett. **94**, 030501 (2005).

[57] N. K. Langford, T. J. Weinhold, R. Prevedel, K. J. Resch, A. Gilchrist, J. L. OBrien, G. J. Pryde, and A. G. White, *Demonstration of a Simple Entangling Optical Gate and Its Use in Bell-State Analysis*, Phys. Rev. Lett. **95**, 210504 (2005).

[58] N. Kiesel, C. Schmid, U. Weber, R. Ursin, and H. Weinfurter, *Linear Optics Controlled-Phase Gate Made Simple*, Phys. Rev. Lett. **95**, 210505 (2005).

[59] R. Okamoto, H. F. Hofmann, S. Takeuchi, and K. Sasaki, *Demonstration of an Optical Quantum Controlled-NOT Gate without Path Interference*, Phys. Rev. Lett. **95**, 210506 (2005).

[60] B. P. Lanyon, M. Barbieri, M. P. Almeida, T. Jennewein, T. C. Ralph, K. J. Resch, G. J. Pryde, J. L. OBrien, A. Gilchrist, A. G. White, *Simplifying quantum logic using higher-dimensional Hilbert spaces*, Nature Physics **5**, 134 (2008).

[61] T. B. Pittman, B. C. Jacobs, and J. D. Franson, *Demonstration of Nondeterministic Quantum Logic Operations Using Linear Optical Elements*, Phys. Rev. Lett. **88**, 257902 (2002).

[62] M. Mičuda, M. Ježek, M. Dušek, and J. Fiurášek, *Experimental realization of a programmable quantum gate*, Phys. Rev. A **78**, 062311 (2008).

[63] A. Černoch, J. Soubusta, L. Bartůšková, M. Dušek, and J. Fiurášek, *Experimental Realization of Linear-Optical Partial swap Gates*, Phys. Rev. Lett. **100**, 180501 (2008).

[64] L. Slodička, M. Ježek, and J. Fiurášek, *Experimental demonstration of a teleportation-based programmable quantum gate*, Phys. Rev. A **79**, 050304(R) (2009).

[65] X.-C. Yao, J. Fiurášek, He Lu1, Wei-Bo Gao1, Yu-Ao Chen1, Zeng-Bing Chen1, and Jian-Wei Pan, *Experimental Realization of Programmable Quantum Gate Array for Directly Probing Commutation Relations of Pauli Operators*, Phys. Rev. Lett. **105**, 120402 (2010).

[66] O. Mandel, M. Greiner, A. Widera, T. Rom, T. W. Hänsch, and I. Bloch, *Controlled collisions for multi-particle entanglement of optically trapped atoms*, Nature **425**, 937 (2003).

[67] M.Anderlini, P. J. Lee, B. L. Brown, J. Sebby-Strabley, W. D. Phillips, and J. V. Porto, *Controlled exchange interaction between pairs of neutral atoms in an optical lattice*, Nature **448**, 452 (2007).

[68] F. Schmidt-Kaler, H. Häffner, M. Riebe, S. Gulde, G. P. T. Lancaster, T. Deuschle, C. Becher, C. F. Roos, J. Eschner, R. Blatt, *Realization of the Cirac-Zoller controlled-NOT quantum gate*, Nature **422**, 408 (2003).

[69] D. Leibfried, B. DeMarco, V. Meyer, D. Lucas, M. Barrett, J. Britton, W. M. Itano, B. Jelenkovi, C. Langer, T. Rosenband, and D. J. Wineland, *Experimental demonstration of a robust, high-fidelity geometric two ion-qubit phase gate*, Nature **422**, 412 (2003).

[70] T. Monz, K. Kim, W. Hänsel, M. Riebe, A. S. Villar, P. Schindler, M. Chwalla, M. Hennrich, and R. Blatt, *Realization of the Quantum Toffoli Gate with Trapped Ions*, Phys. Rev. Lett. **102**, 040501 (2009).

[71] M. Steffen, M. Ansmann, R. C. Bialczak, N. Katz, E. Lucero, R. McDermott, M. Neeley, E. M. Weig, A. N. Cleland, and J. M. Martinis, *Measurement of the Entanglement of Two Superconducting Qubits via State Tomography*, Science **8**, 1423 (2006).

[72] J. H. Plantenberg, P. C. de Groot, C. J. P. M. Harmans, and J. E. Mooij, *Demonstration of controlled-NOT quantum gates on a pair of superconducting quantum bits*, Nature **447**, 836 (2007).

[73] D. G. Cory, A. F. Fahmy, and T. F. Havel, *Ensemble quantum computing by NMR-spectroscopy*, Proc. Natl Acad. Sci. USA **94**, 1634 (1997).

[74] N. A. Gershenfeld and I. L. Chuang, *Bulk spin resonance quantum computation*, Science **275**, 350 (1997).

[75] C. Negrevergne, T. S. Mahesh, C. A. Ryan, M. Ditty, F. Cyr-Racine, W. Power, N. Boulant, T. Havel, D. G. Cory, and R. Laflamme, *Benchmarking Quantum Control Methods on a 12-Qubit System*, Phys. Rev. Lett. **96**, 170501 (2006).

[76] L. M. K. Vandersypen, M. Steffen, G. Breyta, C. S. Yannoni, M. H. Sherwood, and I. L. Chuang, *Experimental realization of Shor's quantum factoring algorithm using nuclear magnetic resonance*, Nature **414**, 883 (2001).

[77] M.A. Nielsen and I. L. Chuang, *Programmable quantum gate arrays*, Phys. Rev. Lett. **79**, 321 (1997).

[78] G. Vidal, L. Masanes, and J. I. Cirac, *Storing quantum dynamics in quantum states: A stochastic programmable gate*, Phys. Rev. Lett. **88**, 047905 (2002).

[79] M. Hillery, V. Bužek, and M. Ziman, *Probabilistic implementation of universal quantum processors*, Phys. Rev. A **65**, 022301 (2002).

[80] M. Hillery, M. Ziman, and V. Bužek, *Implementation of quantum maps by programmable quantum processors*, Phys. Rev. A **66**, 042302 (2002).

[81] M. Hillery, M. Ziman, and V. Bužek, *Improving the performance of probabilistic programmable quantum processors*, Phys. Rev. A **69**, 042311 (2004).

[82] A. Brazier, V. Bužek, and P.L. Knight, *Probabilistic programmable quantum processors with multiple copies of program states*. Phys. Rev. A **71**, 032306 (2005).

[83] M. Hillery, M. Ziman, and V. Bužek, *Approximate programmable quantum processors*, Phys. Rev. A **73**, 022345 (2006).

[84] G.M. D'Ariano and P. Perinotti, *Efficient universal programmable quantum measurements*, Phys. Rev. Lett. **94**, 090401 (2005).

[85] S.M. Barnett, A. Chefles, and I. Jex, *Comparison of two unknown pure quantum states*, Phys. Lett. A **307**, 189 (2003).

[86] G.M. D'Ariano, P. Perinotti, M. F. Sacchi, *Quantum universal detectors*, Europhys. Lett. **65**, 165 (2004), quant-ph/0306025.

[87] M. Dušek and V. Bužek, *Quantum-programled measurement device for quantum-state discrimination*, Phys. Rev. A **66**, 022112 (2002).

[88] J. Fiurášek, M. Dušek, and R. Filip, *Universal Measurement Apparatus programled by Quantum Software*, Phys. Rev. Lett. **89**, 190401 (2002).

[89] J. Fiurášek and M. Dušek, *Probabilistic quantum multimeters*, Phys. Rev. A **69**, 032302 (2004).

[90] J.A. Bergou and M. Hillery, *Universal programmable quantum state discriminator that is optimal for unambiguously distinguishing between unknown states*, Phys. Rev. Lett. **94**, 160501 (2005).

[91] B. He and J. A. Bergou, *Programmable unknown quantum-state discriminators with multiple copies of program and data: A Jordan-basis approach*, Phys. Rev. A **75**, 032316 (2007).

[92] C. Zhang, M. Ying, and B. Qiao, *Universal programmable devices for unambiguous discrimination*, Phys. Rev. A **74**, 042308 (2006).

[93] J. A. Bergou, V. Bužek, E. Feldman, U. Herzog, and M. Hillery, *Programmable quantum-state discriminators with simple programs*, Physical Review A **73**, 062334 (2006).

[94] J. Soubusta, A. Černoch, J. Fiurášek, and M. Dušek, *Experimental realization of a programmable quantum-state discriminator and a phase-covariant quantum multimeter*, Phys. Rev. A **69**, 052321 (2004).

[95] T. Gopinath, R. Das, and A. Kumar, *Programmable quantum-state discriminator by nuclear magnetic resonance*, Phys. Rev. A **71**, 042307 (2005).

[96] M. Sedlák, M. Ziman, O. Přibyla, V. Bužek, and M. Hillery, *Unambiguous identification of coherent states: Searching a quantum database*, Phys. Rev. A **76**, 022326 (2007).

[97] L. Bartůšková, A. Černoch, J. Soubusta, and M. Dušek, *Programmable discriminator of coherent states: Experimental realization*, Phys. Rev. A **77**, 034306 (2008).

[98] R. Raussendorf and H. J. Briegel, *A One-Way Quantum Computer*, Phys. Rev. Lett. **86**, 5188 (2001).

[99] M. A. Nielsen, *Optical Quantum Computation Using Cluster States*, Phys. Rev. Lett. **93**, 040503 (2004).

[100] M. A. Nielsen, *Cluster-state quantum computation*, Rep. Math. Phys. **57**, 147 (2006).

[101] M. Born and E. Wolf, *Principles of Optics*, (Cambridge University Press, Cambridge, 1999).

[102] D. F. Walls and G. J. Milburn, *Quantum Optics*, (Springer-Verlag, New York, 1995).

[103] M. O. Scully and M. S. Zubairy, *Quantum Optics*, (Cambridge University Press, Cambridge, 1997).

[104] O. E. Martínez, *Grating and prism compressors in the case of finite beam size*, J. Opt. Soc. Am. B **3**, 929 (1986).

[105] J. P. Torres, M. W. Mitchell, and M. Hendrych, *Indistinguishability of entangled photons generated with achromatic phase matching*, Phys. Rev. A **71**, 022320 (2005).

[106] I. A. Walmsley and M. G. Raymer, *Toward Quantum-Information Processing with Photons*, Science **307**, 1733 (2005).

[107] L. M. Duan, M. Lukin, J. I. Cirac, and P. Zoller, *Long-distance quantum communication with atomic ensembles and linear optics*, Nature **414**, 413 (2001).

[108] V. Giovannetti, S. Lloyd, and L. Maccone, *Quantum-Enhanced Measurements: Beating the Standard Quantum Limit*, Science **306**, 1330 (2004).

[109] V. Giovannetti, L. Maccone, and S. Lloyd, *Quantum-enhanced positioning and clock synchronization*, Nature **412**, 417 (2001).

[110] A. Valencia, G. Scarcelli, and Y. H. Shih, *Distant clock synchronization using entangled photon pairs*, Appl. Phys. Lett. **85**, 2655 (2004).

[111] T. E. Keller and M. H. Rubin, *Theory of two-photon entanglement for spontaneous parametric down-conversion driven by a narrow pump pulse*, Phys. Rev. A **56**, 1534 (1997).

[112] W. P. Grice and I. A. Walmsley, *Spectral information and distinguishability in type-II down-conversion with a broadband pump*, Phys. Rev. A **56**, 1627 (1997).

[113] G. Di Giuseppe, L. Haiberger, F. De Martini, and A. V. Sergienko, *Quantum interference and indistinguishability with femtosecond pulses*, Phys. Rev. A **56**, R21(1997).

[114] P. J. Mosley, J. S. Lundeen, B. J. Smith, P. Wasylczyk, A. B. URen, Ch. Silberhorn, and I. A. Walmsley, *Heralded Generation of Ultrafast Single Photons in Pure Quantum States*, Phys. Rev. Lett. **100**, 133601 (2008).

[115] O. Kuzucu, M. Fiorentino, M. A. Albota, F. N. C. Wong, and F. X. Kärtner, *Two-Photon Coincident-Frequency Entanglement via Extended Phase Matching*, Phys. Rev. Lett. **94**, 083601 (2005).

[116] M. Hendrych, M. Mičuda, and J. P. Torres, *Tunable control of the frequency correlations of entangled photons*, Opt. Lett. **32**, 2339 (2007).

[117] A. Valencia, A. Ceré, X. Shi, G. Molina-Terriza, and J. P. Torres, *Shaping the waveform of entangled photons*, Phys. Rev. Lett. **99**, 243601 (2007).

[118] O. Cohen, J. S. Lundeen, B. J. Smith, G. Puentes, P. J. Mosley, and I. A. Walmsley, *Tailored Photon-Pair Generation in Optical Fibers*, Phys. Rev. Lett. **102**, 123603 (2009).

[119] J.C. Diels and W. Rudolph, *Ultrashort laser pulse phenomena*, (Academic Press, San Diego, 1995), Chap. 2.6.

[120] J.P. Torres, S. Carrasco, L. Torner, and E.W. VanStryland, *Frequency doubling of femtosecond pulses in walk-off-compensated N-(4-nitrophenyl)-L-prolinol*, Opt. Lett. **25**, 1735 (2000).

[121] M. H. Rubin, D. N. Klyshko, Y. H. Shih, and A. V. Sergienko, *Theory of two-photon entanglement in type-II optical parametric down-conversion*, Phys. Rev. A **50**, 5122 (1994).

[122] M. Hendrych, X. Shi, A. Valencia, and J. P. Torres, *Broadening the bandwidth of entangled photons: A step towards the generation of extremely short biphotons*, Phys. Rev. A **79**, 023817 (2009).

[123] S. Parker, S. Bose, and M. B. Plenio, *Entanglement quantification and purification in continuous-variable systems*, Phys. Rev. A **61**, 032305 (2000).

[124] J. P. Torres, F. Macià, S. Carrasco, and L. Torner, *Engineering the frequency correlations of entangled two-photon states by achromatic phase matching*, Opt. Lett. **30**, 314 (2005).

[125] O. Kuzucu, F. N. C. Wong, S. Kurimura, and S. Tovstonog, *Joint Temporal Density Measurements for Two-Photon State Characterization*, Phys. Rev. Lett. **101**, 153602 (2008).

[126] O. E. Martínez, *Achromatic phase matching for 2nd harmonic-generation of femtosecond pulses*, IEEE J. Quantum Electron. **25**, 2464 (1989).

[127] A. Dubietis, G. Valiulis, G. Tamošauskas, R. Danielius, and A. Piskarskas, *Nonlinear second-harmonic pulse compression with tilted pulses*, Opt. Lett. **22**, 1071 (1997).

[128] P. Di Trapani, D. Caironi, G. Valiulis, A. Dubietis, R. Danielius, and A. Piskarskas, *Observation of temporal solitons in second-harmonic generation with tilted pulses*, Phys. Rev. Lett. **81**, 570 (1998).

[129] X. Liu, L. J. Qian, and F. W. Wise, *Generation of optical spatiotemporal solitons*, Phys. Rev. Lett. **82**, 4631 (1999).

[130] V. Balic, D. A. Braje, P. Kolchin, G. Y. Yin, and S. E. Harris, *Generation of paired photons with controllable waveforms*, Phys. Rev. Lett. **94**, 183601 (2005).

[131] T. B. Pittman, B. C. Jacobs, and J. D. Franson, *Probabilistic quantum logic operations using polarizing beam splitters*, Phys. Rev. A **64**, 062311 (2001).

[132] T. B. Pittman, B. C. Jacobs, and J. D. Franson, *Demonstration of Nondeterministic Quantum Logic Operations Using Linear Optical Elements*, Phys. Rev. Lett. **88**, 257902 (2002).

[133] T. B. Pittman, M. J. Fitch, B. C Jacobs, and J. D. Franson, *Experimental programled-NOT logic gate for single photons in the coincidence basis*, Phys. Rev. A **68**, 032316 (2003).

[134] F. Sciarrino, M. Ricci, F. De Martini, R. Filip, and L. Mišta Jr., *Experimental realization of a minimal disturbance quantum measurement*, Phys. Rev. Lett. **96**, 020408 (2006).

[135] R. Prevedel, P. Walther, F. Tiefenbacher, P. Bohl, R. Kaltenbaek, T. Jennewein, and A. Zeilinger, *High-speed linear optics quantum computing using active feed-forward*, Nature (London) **445**, 65 (2007).

[136] A. Jamiolkowski, *Linear transformations which preserve trace and positive semidefiniteness of operators*, Rep. Math. Phys. **3**, 275 (1972).

[137] M.-D. Choi, *Completely positive linear maps on complex matrices*, Linear Algebr. Appl. **10**, 285 (1975).

[138] A. Černoch, L. Bartůšková, J. Soubusta, M. Ježek, J. Fiurášek, and M. Dušek, *Experimental phase-covariant cloning of polarization states of single photons*, Phys. Rev. A **74**, 042327 (2006).

[139] A. Černoch, J. Soubusta, L. Bartůšková, M. Dušek, and J. Fiurášek, *Experimental realization of linear-optical partial swap gates*, Phys. Rev. Lett. **100**, 180501 (2008).

[140] M. Ježek, J. Fiurášek, and Z. Hradil, *Quantum inference of states and processes*, Phys. Rev. A **68**, 012305 (2003).

[141] Z. Hradil, J. Řeháček, J. Fiurášek, and M. Ježek, *Maximum-likelihood methods in quantum mechanics*, Lect. Notes Phys. **649**, 59 (2004).

[142] Z. Hradil, *Quantum-state estimatio*n, Phys. Rev. A **55**, R1561 (1997).

[143] K. Banaszek, G. M. D'Ariano, M. G. Paris, and M. F. Sacchi, *Maximum-likelihood estimation of the density matrix*, Phys. Rev. A **61**, 010304 (2000).

[144] M. Horodecki, P. Horodecki, and R. Horodecki, *General teleportation channel, singlet fraction, and quasidistillation*, Phys. Rev. A **60**, 1888 (1999).

[145] A. S. Holevo, *Statistical decision theory for quantum systems*, J. Multivar. Anal. **3**, 337 (1973).

[146] C.W. Helstrom, *Quantum detection and estimation theory* (Academic Press, New York, 1976).

[147] A.M. Childs, J. Preskill, and J. Renes, *Quantum information and precision measurement*, J. Mod. Opt. **47**, 155 (2000).

[148] A. Acín, *Statistical distinguishability between unitary operations*, Phys. Rev. Lett. **87**, 177901 (2001).

[149] G. Mauro D'Ariano, M.F. Sacchi, and J. Kahn, *Minimax discrimination of two Pauli channels*, Phys. Rev. A **72**, 052302 (2005).

[150] M.F. Sacchi, *Minimum error discrimination of Pauli channels*, J. Opt. B **7**, S333 (2005); *Optimal discrimination of quantum operations*, Phys. Rev. A **71**, 062340 (2005).

[151] G. Wang and M. Ying, *Unambiguous discrimination among quantum operations*, Phys. Rev. A **73**, 042301 (2006).

[152] Z. Ji, Y. Feng, R. Duan, and M. Ying, *Identification and distance measures of measurement apparatus*, Phys. Rev. Lett. **96**, 200401 (2006).

[153] M. Ziman and T. Heinosaari, *Discrimination of quantum observables using limited resources*, Phys. Rev. A **77**, 042321 (2008).

[154] M. Ziman, T. Heinosaari, and M. Sedlak, *Unambiguous comparison of quantum measurements*, Phys. Rev. A **80**, 052102 (2009).

[155] L. Li and D. Qiu, *Optimal discrimination between quantum operations*, J. Phys. A: Math. Theor. **41**, 335302 (2008).

[156] G. Chiribella, G. M. D'Ariano, and P. Perinotti, *Memory effects in quantum channel discrimination*, Phys. Rev. Lett. **101**, 180501 (2008).

[157] R. Duan, Y. Feng, and M. Ying, *Perfect distinguishability of quantum operations*, Phys. Rev. Lett. **103**, 210501 (2009).

[158] G. M. D'Ariano, P. Lo Presti, and M. G. A. Paris, *Using entanglement improves the precision of quantum measurements*, Phys. Rev. Lett. **87**, 270404 (2001).

[159] G. M. D'Ariano, P. Lo Presti, and M. G. A. Paris, *Improved discrimination of unitaries by entangled probes*, J. Opt. B **4**, 273 (2002).

[160] R. Duan, Y. Feng, and M. Ying, *Entanglement Is Not Necessary for Perfect Discrimination between Unitary Operations*, Phys. Rev. Lett. **98**, 100503 (2007).

[161] X.-F. Zhou, Y.-S. Zhang, and G. C. Guo, *Unitary Transformations Can Be Distinguished Locally*, Phys. Rev. Lett. **99**, 170401 (2007).

[162] R. Duan, Y. Feng, and M. Ying, *Local Distinguishability of Multipartite Unitary Operations*, Phys. Rev. Lett. **100**, 020503 (2008).

[163] M. Piani and J. Watrous, *All entangled states are useful for channel discrimination*, Phys. Rev. Lett. **102**, 250501 (2009).

[164] P. Zhang, L. Peng, Z.-W. Wang, X.-F. Ren, B.-H. Liu, Y.-F. Huang, and G.-C. Guo, *Linear-Optical Implementation of Perfect Discrimination between Single-bit Unitary Operations*, J. Phys. B: At. Mol. Opt. Phys. **41**, 195501 (2008).

[165] A. Laing, T. Rudolph, and J. L. O'Brien, *Experimental Quantum Process Discrimination*, Phys. Rev. Lett. **102**, 160502 (2009).

[166] G. Chiribella, G. M. D'Ariano, and P. Perinotti, *Quantum Circuits Architecture*, Phys. Rev. Lett. **101**, 060401 (2008).

[167] G. Chiribella, G. M. D'Ariano, and P. Perinotti, *A theoretical framework for quantum networks*, Phys. Rev. A **80**, 022339 (2009).